Cell Communication and Signaling

RESEARCH Open Access

The interplay of cancer-associated fibroblasts and apoptotic cancer cells suppresses lung cancer cell growth through WISP-1-integrin αvβ3-STAT1 signaling pathway

Shinyoung Kim[1,2†], Kyungwon Yang[1,2†], Kiyoon Kim[2†], Hee Ja Kim[1], Da Young Kim[1,2], Jeesoo Chae[3], Young-Ho Ahn[2,4] and Jihee Lee Kang[1,2*]

Abstract

Background Cell death within the tumor microenvironment (TME) plays a crucial role in controlling cancer by influencing the balance of tumor-specific immunity. Cancer-associated fibroblasts (CAFs) significantly contribute to tumor progression through paracrine mechanisms. We found that reprogramming of CAFs by apoptotic cancer cells suppresses tumor volume and lung metastasis. Here, we investigated the mechanisms by which the interaction between apoptotic lung cancer cells and CAFs hinders tumor growth.

Methods Experimental methods including CCK assay, colony formation assay, immunoblotting, co-immunoprecipitation, qRT-PCR analysis, qRT-PCR array, apoptosis assay, ELISA, and immunofluorescent staining were used in this study. Additionally, CAFs were isolated from lung tumors of Kras-mutant (*Kras*LA1) mice and human lung adenocarcinoma samples using magnetic-activated cell sorting. Murine lung cancer cells (344SQ cells) along with various human cancer cell lines (A549, HCT116, and LoVo) were cultured. In animal study, conditioned medium (CM) derived from CAFs (undiluted or 50% diluted) with or without neutralizing anti-WISP-1 antibody was administered into syngeneic mice to study anti-tumoral effects. To confirm the paracrine role of WISP-1, recombinant WISP-1 (rWISP-1) was administered via intratumoral injection.

Results We demonstrate that treatment with CM from lung CAFs exposed to apoptotic cancer cells suppresses proliferation and promotes apoptosis in lung cancer cells through STAT1 signaling. Pharmacologic inhibition of Notch1 activation or siRNA-mediated Notch1 silencing in CAFs reversed the antiproliferative and proapoptotic effects. Similarly, knockdown of Wnt-induced signaling protein 1 (WISP-1) in CAFs or neutralizing the CM with anti-WISP-1 antibodies reversed the antiproliferative and proapoptotic effects. WISP-1 signaled through integrin αvβ3-STAT1 signaling pathway to inhibit cancer cell growth and promote apoptosis. The in vivo introduction of

†Shinyoung Kim, Kyungwon Yang and Kiyoon Kim contributed equally to this work.

*Correspondence:
Jihee Lee Kang
jihee@ewha.ac.kr

Full list of author information is available at the end of the article

CM derived from apoptotic 344SQ-exposed CAFs (ApoSQ-CAF CM) potently decelerated tumor growth. This effect was observed alongside the downregulation of proliferative and anti-apoptotic markers, while simultaneously boosting the activation of phosphorylated STAT1 and pro-apoptotic markers in $CD326^+$ tumor cells within syngeneic immunocompetent mice. rWISP-1 effectively replicates the in vivo effects of ApoSQ-CAF CM.

Conclusions These findings suggest that CM from apoptotic cancer cell-exposed CAFs may offer a promising therapeutic approach by lung cancer suppression.

Keywords CAF, Apoptotic cancer cell, Lung cancer, WISP-1-integrin αvβ3-STAT1 signaling pathway, Tumor growth

Introduction

Lung cancer ranks as the leading cause of cancer-related death in men and the second leading cause in women worldwide [1]. Despite significant advances in diagnostic and genetic technologies, surgical techniques, and novel biological treatments, the 5-year survival rate for lung cancer patients remains dismally low at 18.6% [2], with over half succumbing within the first year of diagnosis. Identifying prognostic factors is crucial to assess treatment effectiveness and optimize survival outcomes [3].

Cancer growth, progression, therapy resistance, invasion, and metastasis are intricately influenced by bidirectional interactions between cancer cells and their environment, thus shaping the tumor microenvironment (TME) [4]. Nonprofessional phagocytes known as cancer-associated fibroblasts (CAFs) are the predominant cell type within the tumor stroma, exhibiting migratory and contractile properties akin to myofibroblasts. CAFs produce a range of molecules, including chemokines, cytokines, growth factors, miRNAs, exosomes, and metabolites, to orchestrate the malignant biology of cancer cells and other TME components [5, 6]. Notably, CAFs play pivotal roles in promoting primary tumor development, growth, and progression by fostering neoangiogenesis and stimulating tumor cell proliferation, survival, migration, and invasion [6]. Targeting CAFs and their interactions within the TME holds significant promise for improving malignant tumor treatment. However, the clinical application of CAF inhibitors faces numerous challenges due to the heterogeneous nature of CAFs, stemming from their diverse origins and multifaceted functions that encompass both pro-and anti-tumorigenic roles within tumors [7, 8].

Cell death in the TME profoundly affects tumor-specific immunity [9], shaping its overall immune balance. Apoptotic cell clearance (efferocytosis), coupled with cytokine modulation involved in wound healing and immune suppression, may promote cancer progression by allowing cancer cells to evade immune surveillance within the TME [10, 11]. Conversely, our previous work demonstrated that CAF-mediated efferocytosis of apoptotic lung cancer cells suppresses migration and invasion of both cancer cells and CAFs. This suppression occurs through the secretion of Wnt-induced signaling protein 1 (WISP-1), also known as cellular communication network factor 4 (CCN4), in paracrine and autocrine manners [12]. Injection of conditioned medium (CM) from apoptotic lung cancer cell-exposed CAFs reduced tumor volume and lung metastasis, indicating a role in inhibiting neoplastic progression [13].

However, despite this understanding, the precise mechanisms by which the interaction between apoptotic lung cancer cells and CAFs hinders tumor growth remain poorly characterized. Here, we demonstrate that the interaction of CAFs with apoptotic lung cancer cells effectively reduces lung cancer cell proliferation and intensifies apoptosis through WISP-1 release. As a paracrine mechanism, the WISP-1-integrin αvβ3-signal transducer and activator of transcription 1 (STAT1) signaling pathways play essential roles in the antiproliferative and pro-apoptotic effects in lung cancer cells. Furthermore, we provide in vivo evidence that intratumoral injection of CM obtained from CAFs exposed to apoptotic lung cancer cells mediates the anti-tumor growth effect through the WISP-1-STAT1 signaling pathway.

Materials and methods

Reagents

Fludarabine was purchased from Tocris Bioscience (Bristol, UK). LY3039478 (HY-12449) was purchased from MedChemExpress (Monmouth Junction, NJ, USA). Mouse recombinant WISP-1 (rWISP-1) (1680-WS), human rWISP-1 (1627-WS), neutralizing mouse WISP-1 antibodies (MAB1680), and IgG (MAB0061) were purchased from R&D Systems (Minneapolis, MN, USA).

CAF isolation and cell culture

CAFs were isolated from lung tumors of Kras-mutant (*Kras*LA1) mice using magnetic-activated cell sorting with the fibroblast-specific marker Thy1 as previously described [12, 14]. In our prior investigation, we demonstrated that $Thy1^+$ CAFs exhibits smaller surface areas and elongated spindle shapes, which are regarded as a typical characteristic of activated fibroblasts, compared with normal lung fibroblasts [14]. Human $Thy1^+$ CAFs (*h*CAFs) were isolated from untreated, primary, nonmetastatic lung tumors [15]. CAFs were then cultured in alpha-minimum essential medium

supplemented with 10% fetal bovine serum (FBS), penicillin/streptomycin (100 U/100 μg), 2 mM L-glutamine (Welgene, Gyeongsan, Korea), and 1 mM sodium pyruvate (Welgene). Human cancer cell lines were procured from the American Type Culture Collection (ATCC, Manassas, VA). 344SQ cells (a gift from Dr. Jonathan M. Kurie, University of Texas MD Anderson Cancer Center, Houston, TX, USA) along with various human cancer cell lines [A549 (lung), HCT116, and LoVo (colon)] were maintained in RPMI 1640 (HyClone™, GE Healthcare, Boston, MA, USA) supplemented with 10% FBS and penicillin/streptomycin (100 U/100 μg).

Induction of cell death

Cancer epithelial cell lines were exposed to ultraviolet irradiation at 254 nm for 15 min, followed by incubation in RPMI-1640 supplemented with 10% FBS for 2 h at 37 °C and 5% CO_2. Assessment of nuclear morphology using light microscopy on Wright-Giemsa-stained samples reveals apoptotic features in irradiated cells [16]. Lysed (necrotic) cancer cells were obtained through multiple freeze-thaw cycles. The occurrence of apoptosis and necrosis was confirmed through Annexin V-FITC/propidium iodide (PI) staining (BD Biosciences, San Jose, CA, USA) followed by flow cytometric analysis conducted on a FACSCalibur system (BD Biosciences) [12, 16].

Preparation of CAF CM

CAFs were plated at 3×10^5 cells/ml and cultured at 37 °C and 5% CO_2. Following overnight incubation, cells were serum-starved using X-VIVO 10 medium (04-380Q, Lonza, Basel, Switzerland) for 24 h before cell stimulation. For stimulation, the culture medium was replaced with X-VIVO 10 containing apoptotic or necrotic cancer cells (9×10^5 cells/ml). After 20 h, the medium was collected and centrifuged at 2000 *g* for 20 min in order to remove cell remnants and apoptotic bodies. The supernatant was then filtered through 220 nM pore filter, and then used as the CM for stimulating target cancer epithelial cells (5×10^3 cells/ml). For in vivo experiments, CM was stored at -80 °C until required.

Cell viability assay

Cancer cells (5×10^3) were plated into 96-well plates (SPL, Pocheon, Korea) with RPMI-1640 or X-VIVO 10 medium (Lonza, Basel, Switzerland) for 6 h. CM or rWISP-1 was added to each group. Plates were incubated at 37 °C with 5% CO_2 for 1–5 days. Subsequently, Cell Counting Kit-8 (CCK-8) solution (Dojindo Molecular Technologies, Rockville, MD, USA) was added to the wells, and the plates were further incubated at 37 °C with 5% CO_2 for 30 min. Absorbance was measured at 450 nm using a microplate reader.

Colony formation assay

Cancer cells were seeded at 500 cells/well in 6-well plates (SPL Life Sciences, Pocheon-si, Gyeonggi-do, Korea) with X-VIVO 10 (control) or CM. Plates were incubated at 37 °C with 5% CO_2 for 8–9 days, with medium changes every 4 days. Formed colonies were fixed with 95% ethanol at 4 °C overnight and subsequently stained with 0.1% crystal violet (Sigma-Aldrich, St Louis, MO, USA) diluted in 20% methanol at room temperature overnight. Following plate washing, visible colonies containing greater than 50 cells were counted from 5 fields using a stereomicroscope. Representative colonies were imaged, and three independent experiments were conducted.

Immunoblotting analysis

Standard Western blots were conducted using whole-cell extracts obtained from lung cancer cells. Cells were harvested, washed with ice-cold phosphate-buffered saline (PBS), and lysed in radioimmunoprecipitation assay buffer [10 mM Tris (pH 7.2), 150 mM NaCl, 1% Nonidet P-40, 0.5% sodium deoxycholate, 0.1% SDS, 1.0% Triton X-100, and 5 mM EDTA], supplemented with protease inhibitors, for 30 min on ice. Equivalent amounts of protein were separated on SDS-PAGE gels (#161 – 0158, Bio-Rad Laboratories, Hercules, CA, USA) and transferred to nitrocellulose membranes (10600001, GE Healthcare Life Science, Piscataway, NJ, USA) using a wet transfer system (Bio-Rad Laboratories). Following blocking with 5% bovine serum albumin (BSA)-TBST or 5% milk-TBST for 1 h, the membranes were incubated overnight with the appropriate primary antibodies, followed by incubation with the corresponding secondary antibody for 1 h at 37 °C. The blots were developed using an enhanced chemiluminescence detection kit (Thermo Fisher Scientific, Waltham, MA, USA). Protein bands were visualized using a ImageQuant LAS 4000 mini (GE Healthcare, Chicago, IL, USA) or Amersham ImageQuant 800 (Cytiva, Marlborough, MA, USA). For quantification, the density of specific target bands was normalized against β-actin using ImageJ software, version 1.37 (National Institutes of Health, Bethesda, MD, USA). Antibody information is provided in Table S1.

Co-immunoprecipitation (CoIP)

Lung cancer cells were lysed with lysis buffer (50mM Tris-HCl pH7.8, 137mM NaCl, 1mM EDTA, 1% Triton X-100, 10% glycerol and protease inhibitor cocktail) and pre-cleared by centrifugation at 14,000 rpm for 15 min. Cell lysates were incubated with WISP-1 or IgG antibody (1ug) for overnight at 4 °C. After incubation, Protein-A/G conjugated agarose beads (Santa Cruz, sc-2003) were added for 4 h at 4 °C. The precipitations were washed 3 times with lysis buffer. Immunopellets were boiled with SDS-PAGE sample buffer(50mM Tris-HCL pH = 6.8,

2% SDS, 10% glycerol, 1% β-mercapotoethanol, 0.1% bromophenol blue) at 95 °C for 10 min and analyzed by immunoblotting.

Quantitative reverse transcription-PCR (qRT-PCR)

Total RNA was extracted from cancer cells utilizing TRIzol reagent (RNAiso plus, Takara Bio Inc., Kusatsu, Japan), and cDNA synthesis was conducted using AccuPower RT PreMix (Bioneer, Daejeon, Korea) following the manufacturer's instructions. SYBR Green–based qRT-PCR was conducted using a QuantStudio™ 3 Real-Time PCR System (Applied Biosystems, Foster City, CA, USA). mRNA levels were normalized to hypoxanthine-guanine phosphoribosyltransferase mRNA and presented as a fold-change in expression compared to the control group. Primer sequences are listed in Table S2.

Transient transfection

CAFs and lung cancer cells were transiently transfected with specific siRNAs targeting WISP-1 (Bioneer), Notch1 (Bioneer), STAT1 (Bioneer), or control siRNA (SN-1003 AccuTarget™ Negative Control; Bioneer) at a final concentration of 50 nM using Lipofectamine RNAi MAX (Invitrogen, Carlsbad, CA) as per the manufacturer's instructions. Following overnight transfection, cells were cultured for 24 h and subsequently stimulated with apoptotic cancer cells. The siRNA sequences are listed in Table S3.

For gene overexpression experiments, 344SQ cells were seeded at 2×10^5 cells/ml in 12-well plates overnight. To overexpress STAT1, cells were transfected with 1 μg of mouse STAT1 gene open reading frame cRNA clone-expression plasmid (Invitrogen) using Lipofectamine 2000 (Thermo Fisher Scientific, Waltham, MA, USA) for 24 h following the manufacturer's instructions. Mock-transfected cells were transfected with the control vector pcDNA3. STAT1 gene and protein expression were assessed in cell lysates to confirm plasmid efficacy.

Apoptosis assay

For the apoptosis assay, an Annexin V-FITC/PI staining kit (BD Biosciences) was utilized according to the manufacturer's instructions. Cells positive for Annexin V-FITC were detected using flow cytometry (ACEA NovoCyte, San Diego, CA, USA). Data analysis was conducted using NovoExpress software 1.5.

Additionally, lung cancer cells and primary tumor tissues were stained using a TUNEL kit (Roche, Basel, Switzerland) following the manufacturer's instructions. Apoptotic cells were visualized using a confocal microscope (LSM5 PASCAL) equipped with a filter set with excitation wavelengths of 488 and 543 nm. Quantitative analysis of TUNEL-positive cells was performed by manually counting the number of TUNEL-positive cells per field in five randomly selected high-power fields per section in a blinded manner; values were averaged for each mouse.

Neutralization of WISP-1 in CM

The CM obtained from CAFs was incubated for 2 h with either 10 μg/ml of mouse anti-mouse WISP-1 neutralizing antibody (R&D Systems) or 10 μg/ml IgG isotype control (R&D Systems). The efficacy of anti-WISP-1 antibody neutralization was assessed by WISP-1 ELISA before utilization.

Enzyme-linked immunosorbent assay (ELISA)

WISP-1 in CM was measured using ELISA kits (R&D Systems) following the manufacturer's instructions.

Mouse experiments

The Animal Care Committee of the Ewha Medical Research Institute approved the experimental protocol for this study (EWHA MEDIACUC 22-015-3). Mice were cared for following the guidelines outlined in the National Institute of Health Guide for the Care and Use of Laboratory Animals.

Subcutaneous syngeneic tumor models were generated by subcutaneously injecting the right posterior flank of 8 week-old male syngeneic (129/Sv) mice ($n = 6–9$ per group) with 344SQ cells (1×10^6 cells in 100 μl of PBS per mouse) [12, 16]. Starting 2 days later, an equal volume of CM derived from CAFs (undiluted or 50% diluted) was administered via intratumoral injection three times per week. Undiluted CM with or without 10 μg/ml neutralizing mouse anti-WISP-1 antibody or isotype IgG was administered following the same schedule ($n = 6$ mice per group). In addition, rWISP-1 was administered via intratumoral injection at doses of 12.5 and 25 μg/kg, three times a week, beginning 2 days after 344SQ injection ($n = 6$ mice per group) [12]. For fludarabine treatment, 120 μl of 10 mg/kg fludarabine solution, prepared in 5% DMSO, 40% PEG300, 5% Tween 80, and 50% ddH2O, was administrated via intraperitoneal injection 1 h before the injection of 25 μg/kg rWISP-1 [17]. Mice were monitored daily for tumor growth and were sacrificed at 6 weeks after injection. Necropsies were performed to measure the diameters and weights of subcutaneous tumor masses.

Tumor volume calculation

Tumor volume was determined using the formula (L × W × W) ÷ 2, where L represents the longer dimension of the tumor and W represents the shorter dimension of the tumor.

Isolation of CD326+ tumor cells from primary tumors

Isolation of single cells from mouse tumors was conducted following a previously described method with slight modifications [18]. Freshly necropsied tumors were digested with RPMI 1640 containing 1× collagenase/hyaluronidase supplemented with 4 U/ml DNase I. Cell suspensions were filtered using 70- and 40-μm sterile nylon mesh and subsequently incubated with red blood cell lysis buffer. After pulse-centrifugation, the non-clear supernatant was collected for macrophage isolation, and the remaining pellets were further digested using dissociation buffer (TrypeLE Express Enzyme supplemented with 4 U/ml DNase I) for cancer cell isolation. $CD326^+$ tumor cells were isolated using CD326 MicroBeads (Miltenyi Biotec, Auburn, CA, USA). Isolated tumor cells were cultured in complete media: RPMI 1640 containing 10% FBS with 1% penicillin-streptomycin for $CD326^+$ cells. The identity of isolated cell populations was confirmed using qRT-PCR. Individual cells were isolated from two or three randomly selected mouse primary tumors in each group.

qRT-PCR arrays

To profile the expression of genes associated with apoptosis and cell cycle arrest in isolated $CD326^+$ tumor cells, we utilized Mouse Cell Cycle RT2 Profiler™ PCR Arrays (PAMM-020ZA, Qiagen, Hilden, Germany) and Mouse Apoptosis RT^2 Profiler™ PCR Arrays (PAMM-012ZA, Qiagen). RNA isolation, DNase treatment, and RNA cleanup were performed according to the manufacturer's instructions (Invitrogen). Isolated RNA was reverse transcribed into cDNA using an RT^2 First Strand Kit (Qiagen). PCR was conducted using RT^2 SYBR Green qPCR Master Mix (Qiagen) on a QuantStudio™3 Real-Time PCR System and ABI PRISM 7900 instrument (Applied Biosystems). Expression data were normalized to the average Ct values of glyceraldehyde 3-phosphate dehydrogenase, as the housekeeping gene in the array. Each assay was performed in triplicate.

Immunofluorescent staining

344SQ cells (10^6 cells/well) cultured on glass coverslips until confluent were fixed in 4% paraformaldehyde for 8 min at room temperature. For staining of paraffin-embedded tumor samples, formalin fixation was performed at room temperature for 30 min, followed by immunofluorescent-wash buffer (0.05% NaN3, 0.1% BSA, 0.2% Triton X-100, and 0.05% Tween-20 in PBS). After fixation, samples were washed three times with wash buffer for 5 min each and permeabilized with 0.5% Triton X-100 (Sigma-Aldrich) in PBS at room temperature for 5 min.

For immunohistochemistry, 5% BSA in PBS was used, whereas, for immunocytochemistry, 5% BSA in PBS with or without mouse IgG blocking reagent was employed. Following a 1-h blocking step, target proteins were labeled with respective primary antibodies during an 18-h incubation at 4 °C. Detected proteins were visualized using fluorescence-conjugated IgG in a dark room for 1 h. Slides were mounted with VECTASHIELD mounting medium containing DAPI (Vector Laboratories, Burlingame, CA, USA) and imaged using a confocal microscope (LSM5 PASCAL, Carl Zeiss, Jena, Germany). Information regarding antibody sources and dilutions is provided in Table S1.

Statistics

Pairwise comparisons were conducted using two-tailed Student's *t*-tests. Analysis of variance was used to perform multiple comparisons, and when necessary, Tukey's post hoc test was used. P values < 0.05 were considered statistically significant. All statistical analyses were performed using Prism 5 software (GraphPad Software Inc., San Diego, CA, USA). Pearson correlation analysis was employed for simple linear correlation analyses.

Results

The interaction between CAFs and apoptotic cancer cells reduces cancer cell proliferation

In our in vitro study, we investigated how the interplay between CAFs and apoptotic cancer cells influences cancer cell growth through paracrine signaling. To address this question, we isolated murine lung CAFs using magnetic-activated cell sorting from the lung tumors of Kras-mutant (*Kras*LA1) mice using Thy-1, a fibroblast-specific marker [12, 14]. $Thy1^+$ CAFs were found to enhance cancer cell invasion and migration in both human and murine models of lung adenocarcinoma [14, 19]. CAFs were treated for 20 h with UV-irradiated apoptotic 344SQ cells (ApoSQ) or necrotic 344SQ cells (NecSQ). Murine 344SQ lung adenocarcinoma cells were treated with CM from CAFs alone (CAF CM) or CAFs exposed to apoptotic 344SQ cells (ApoSQ-CAF CM) or necrotic cells (NecSQ-CAF CM) for 1–5 days. Cell viability was assessed using CCK-8. ApoSQ-CAF CM substantially decreased cancer cell viability after 2–5 days, whereas CAF CM or NecSQ-CAF CM did not (Fig. 1a). This antiproliferative effect was confirmed in human cancer cell lines, including A549 (non-small cell lung cancer), HCT116, and LoVo (both colon cancer), exposed to CM from different types of apoptotic cancer cells (Fig. S1a–c). We further examined the cross-activity of the CM. Treating 344SQ cells with ApoA-CAF CM (CM from CAFs exposed to apoptotic A549 cells), A549 cells with ApoSQ-CAF CM, or HCT116 cells with ApoA-CAF CM also resulted in decreased cell viability (Fig. S1d–f). These findings suggest that the CM exhibits cross-activity, exerting its antiproliferative effect across both human

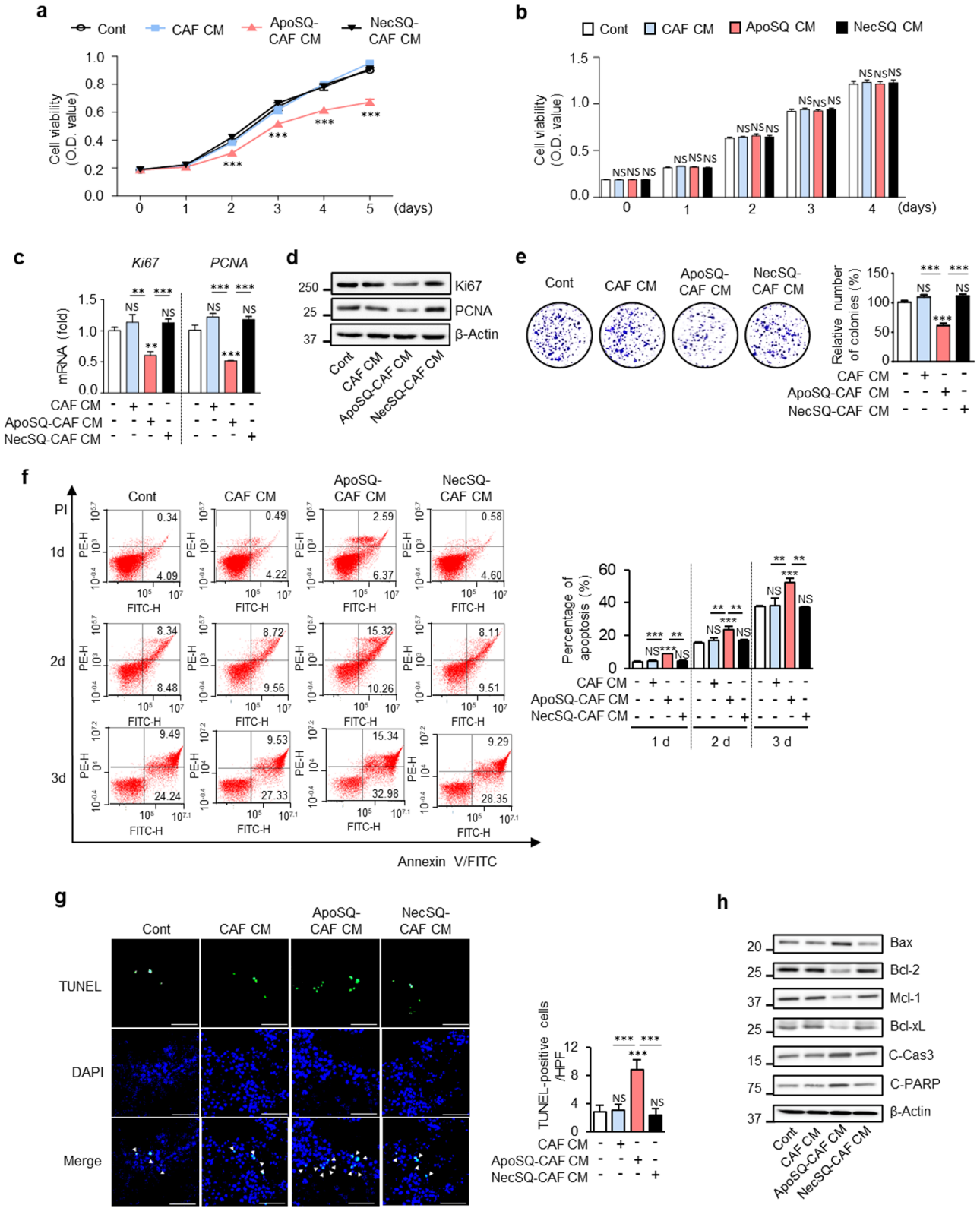

Fig. 1 (See legend on next page.)

(See figure on previous page.)

Fig. 1 Conditioned medium from apoptotic cancer-exposed CAFs inhibits growth of lung cancer cells. (**a**, **b**) Cell viability assay of 344SQ cells. (**a**) CAFs were exposed to apoptotic 344SQ (ApoSQ) or necrotic 344SQ cells (NecSQ) for 20 h. Conditioned medium from CAF only (CAF CM), exposed to ApoSQ (ApoSQ-CAF CM) or NecSQ (NecSQ-CAF CM) was treated to 344SQ cells for the indicated days. (**b**) CAF CM, CM from ApoSQ only (ApoSQ CM), or CM from NecSQ only (NecSQ CM) was added to 344SQ cells for the indicated days. (**c**) qRT-PCR analysis of Ki67 and PCNA in 344SQ samples. (**d**) Immunoblot analysis of the indicated proteins in 344SQ cell lysates. (**e**) *Left*: Representative images of colonies formed by 344SQ cells. *Right*: Quantitation of colony number formed by 344SQ cells. CAF CM, ApoSQ-CAF CM or NecSQ-CAF CM was treated to 344SQ cells for 3 (**c**, **d**) or 8 days (**e**). (**f**) *Left*: Flow cytometry analysis after Annexin V – FICT/PI dual staining was employed to evaluate the cell apoptosis of 344SQ cells. *Right*: Apoptotic cells were quantified as the sum of the percentages of early and late stages of apoptosis. (**g**) Representative images of apoptosis in 344SQ cells by TUNEL assay (original magnification: x200). Nuclei were observed by DAPI staining. Scale bar = 100 μm. *Below*: Quantitation of the number of TUNEL – positive cells (number/HPF) in the different groups. (**h**) Immunoblot analysis of Bax, Bcl-2, Mcl-1, Bcl-xL, cleaved caspase-3, cleaved PARP, and β-actin in 344SQ cell lysates. 344SQ cells were treated with CAF CM, ApoSQ-CAF CM, or NecSQ-CAF CM for 1–3 days for measuring apoptosis by flow cytometry, and 3 days for immunoblot assay. NS, not significant; $^{**}P < 0.01$, $^{***}P < 0.001$, two-tailed Student's *t* test. Data are from one experiment representative of three independent experiments with similar results (**d**, **h**; **e-*gleft***) or from three independent experiments (mean ± standard error: **a-c**; **e-*gright***)

and mouse cells as well as other cancer cell lines. Importantly, CM from apoptotic or necrotic cancer cells alone did not affect cell viability (Fig. 1b and Fig. S1g–i). Next, we explored whether this antiproliferative effect depends on direct contact between CAFs and apoptotic lung cancer cells. We used a transwell system to co-culture CAFs with apoptotic 344SQ cells without direct contact. ApoSQ or ApoA were seeded in the upper wells, while CAFs were seeded in the lower wells and cultured for 20 h. Treatment with CM from CAFs indirectly exposed to ApoSQ or ApoA into the corresponding cancer cells did not affect cell viability (Fig. S1j, k). These data suggest that direct contact between CAFs and apoptotic lung cancer cells is necessary to achieve this antiproliferative effect. Moreover, ApoSQ-CAF CM and ApoA-CAF CM markedly reduced mRNA and protein expression levels of proliferation markers, including Ki-67 and proliferating cell nuclear antigen (PCNA), in the corresponding cancer cells (Fig. 1c, d and Fig. S1l, m). However, CAF CM, NecSQ-CAF CM, and NecA-CAF CM did not affect mRNA and protein expression levels of these proliferation markers.

To further validate the impact of CAF CM on cancer cell proliferation, we examined colony formation. The colony formation assay, an in vitro clonogenic cell survival assay based on a single cell's ability to form a colony, demonstrated that, over 8–9 days, ApoSQ-CAF CM and ApoA-CAF CM inhibited colony formation of 344SQ and A549 cells, respectively (Fig. 1e and Fig. S1n). However, CAF CM, NecSQ-CAF CM, and NecA-CAF CM did not affect colony formation.

Additionally, we investigated the antiproliferative effects of CM from ApoA-exposed *h*CAFs isolated from primary lung tumors [15]. As expected, ApoA-*h*CAF CM reduced cell viability and inhibited colony formation of A549 cells (Fig. S1o, p). However, neither *h*CAF CM nor NecA-*h*CAF CM affected cell viability or colony formation.

The interaction between CAFs and apoptotic cancer cells promotes apoptosis in lung cancer cells

Because CM from CAFs exposed to apoptotic lung cancer cells inhibited lung cancer cell growth, we investigated its effect on apoptosis. ApoSQ-CAF CM and ApoA-CAF CM increased apoptosis at 1, 2, and 3 days, as indicated by Annexin V-FITC-propidium iodide (PI) staining, compared to control media. Conversely, CAF CM, NecSQ-CAFCM, and NecA-CAFCM did not induce apoptosis (Fig. 1f and Fig. S2a). Similarly, terminal deoxynucleotidyl transferase dUTP nick end labeling (TUNEL) assays revealed an increase in TUNEL-positive cells 2 days after ApoSQ-CAF CM and ApoA-CAF CM treatment, whereas CAF CM, NecSQ-CM, and NecA-CM showed no effect (Fig. 1g and Fig. S2b).

For a detailed analysis of apoptosis, we explored caspase-3 activity and pro-apoptotic/anti-apoptotic proteins using Western blot analysis. ApoSQ-CAF CM and ApoA-CAF CM treatment of lung cancer cells increased apoptosis biomarker expression, including Bax, cleaved caspase-3, and cleaved PARP (poly ADP-ribose polymerase), and decreased expression of anti-apoptotic biomarkers such as Bcl-2, Mcl-1, and Bcl-xL (Fig. 1h and Fig. S2c). In contrast, CAF CM NecSQ-CM, and NecA-CM had minimal effects. These results confirm that CM from apoptotic lung cancer cell-exposed CAFs induces lung cancer cell apoptosis, thereby disrupting proliferation.

Notably, ApoA-*h*CAF CM treatment of A549 cells also increased apoptosis at 3 days, compared to control media. Conversely, *h*CAF CM and NecA-*h*CAF CM did not influence apoptosis (Fig. S2d).

ApoSQ-CAF CM injection slows tumor growth *in vivo*

To assess the in vivo anti-tumor effect of paracrine secretions from CAFs exposed to apoptotic cancer cells, undiluted or 50% diluted CAF CM or ApoSQ-CAF CM was intratumorally administered thrice weekly in syngeneic (129/Sv) immunocompetent mice, beginning 2 days after 344SQ injection. Tumor volume was measured at least weekly (Fig. 2a). Although body weight did not significantly differ between treatment groups (Fig. 2b), primary tumor weight decreased markedly (Fig. 2c, d), as did

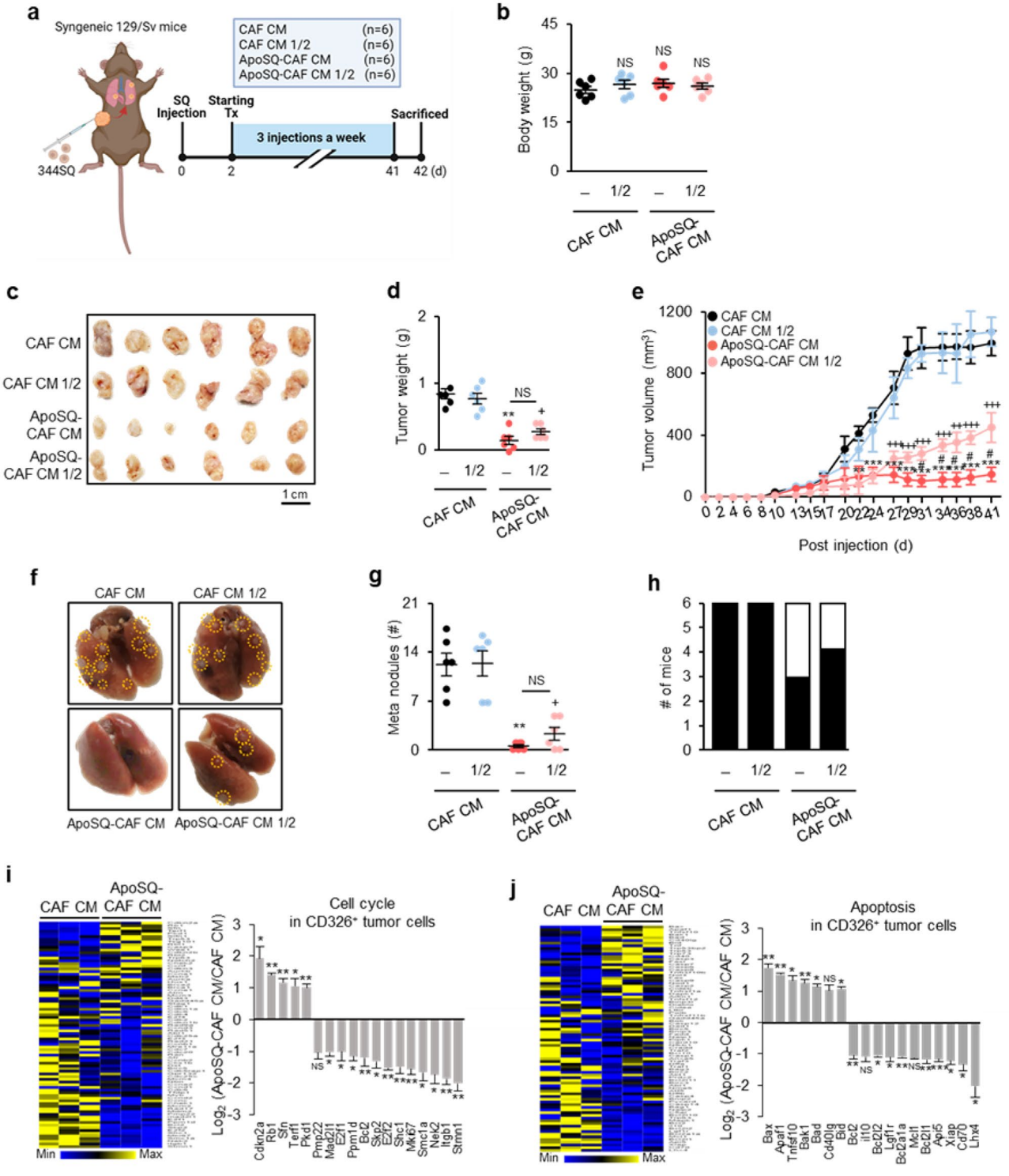

Fig. 2 (See legend on next page.)

(See figure on previous page.)

Fig. 2 Dilution of ApoSQ-CAF CM diminishes anti-tumor growth and anti-metastatic effects in mice. (**a**) Schematic of experimental design and groups. CAF CM, CAF CM (50% dilution with serum free media), ApoSQ-CAF CM, or ApoSQ-CAF CM (50% dilution with serum free media) was intratumorally injected three times a week for 6 weeks starting 2 days after subcutaneous injection of 344SQ cells into syngeneic (129/Sv) mice ($n = 6$ mice per group). Mice were necropsied 6 weeks later. Scatter plots of body weight (**b**), primary tumor weight (**d**), and numbers of lung metastatic nodules (**g**). (**c**) Representative images of primary tumors. (**e**) Tumor volume was measured at the indicated days. (**f**) Representative images of lungs with or without metastatic tumor nodules. The yellow dashed circles indicate lung metastatic nodules. (**h**) Numbers of mice with (w/) and without (w/o) visibly determined metastases (Met). NS, not significant; $^{**}P < 0.01$, $^{***}P < 0.001$ for ApoSQ-CAF CM vs. CAF CM; $^{+}P < 0.05$, $^{+++}P < 0.001$ for ApoSQ-CAF CM 1/2 vs. CAF CM 1/2; $^{\#}P < 0.05$ for ApoSQ-CAF CM vs. ApoSQ-CAF CM 1/2, Analysis of variance with Tukey's post hoc test. The data are presented as the mean ± standard error of results from 6 mice per group. (**i**, **j**) Heatmap showing differentially expressed genes encoding cell cycle- and apoptosis pathway-related molecules in $CD326^{+}$ tumor cells isolated from primary tumors (*left*). Yellow: high expression; blue: low expression. Relative expression of selected genes from PCR array profiling of cell cycle (*right*). Log2 fold-change values (ApoSQ-CAF CM vs. CAF CM). NS, not significant; $^{*}P < 0.05$, $^{**}P < 0.01$, $^{***}P < 0.01$ two-tailed Student's *t*-test. The data are from three replicates per condition with cells pooled from two or three mice per replicate (mean ± standard error: **i** and ***jright***)

tumor growth (Fig. 2e) compared to those treated with CAF CM (undiluted or 50% dilution). Mice treated with ApoSQ-CAF CM (undiluted or 50% dilution) showed significantly fewer tumor nodules on the lung surface and a decreased metastatic rate compared to those treated with CAF CM (undiluted or 50% dilution) (Fig. 2f–h). Notably, 50% diluted ApoSQ-CAF CM yielded less favorable outcomes than undiluted ApoSQ-CAF CM, resulting in reduced tumor volume (approximately 54% vs. 86% inhibition at 41 days) and metastasis rate (approximately 34% vs. 51% inhibition).

To understand the mechanisms underlying the reduction of tumor cell proliferation by ApoSQ-CAF CM in vivo, we analyzed 84 cell cycle genes using a targeted qRT-PCR array. Thirteen cell cycle/mitosis–related genes, including *Stmn1*, *Itgb1*, *Nek2*, *Smc1a*, *Mki67*, *Shc1*, and *E2f2*, were downregulated by more than 2 fold in isolated $CD326^{+}$ tumor cells from the ApoSQ-CAF CM group compared with the CAF CM group (Fig. 2i). Conversely, five cell cycle arrest–related genes, including *Cdkn2a*, *Rb1*, and *Sfn*, were upregulated (> 2 fold) in the ApoSQ-CAF CM group compared with the CAF CM group.

Furthermore, to evaluate the pro-apoptotic effects of ApoSQ-CAF CM at the gene level in vivo, we used a Mouse Apoptosis Pathway RT^{2} Profiler PCR Array to assess the expression of 84 apoptosis-associated genes. Injection of ApoSQ-CAF CM reduced expression levels of 11 genes (> 2 fold) involved in anti-apoptosis, including *Lhx4*, *Cd70*, *Xiap*, *Api5*, and *Bcl2l1*, and upregulated the expression of 7 genes (> 2 fold) involved in pro-apoptosis, including *Bax*, *Apaf1*, and *Tnfs10*, in isolated $CD326^{+}$ tumor cells (Fig. 2j). These findings collectively suggest that paracrine secretion from CAFs stimulated by apoptotic cancer cells inhibits tumor growth, leading to a reduction in metastasis rates.

The antiproliferative and pro-apoptotic effects are mediated through STAT1 signaling

In various contexts, STAT1 exhibits both pro-apoptotic and antiproliferative activities in tumor cells [20]. STAT1-deficient mice are more susceptible to tumor development than those with wild-type STAT1 [21]. Thus, we investigated whether STAT1 activation influences these activities induced by ApoSQ-CAF CM or ApoA-CAF CM. STAT1 phosphorylation (tyrosine 701) showed rapid enhancement within 30 min and persisted for 2 h (Fig. 3a). Alongside alterations in apoptosis-related markers (Fig. 1h), ApoSQ-CAF CM notably enhanced p53 phosphorylation and the expression of p53 and $p21^{Waf1/Cip1}$ (p21) proteins in 344SQ cells compared with CAF CM or NecSQ-CAF CM. p53 and p21 are downstream molecules of STAT1 signaling involved in regulating cell cycle arrest and apoptosis [22, 23]. Similarly, treatment of A549 cells with ApoA-*h*CAF CM also elevated STAT1 phosphorylation and p21 protein expression (Fig. S3a). Immunofluorescent staining and image analysis revealed enhanced staining of phosphorylated STAT1 and p21 in 344SQ cells treated with ApoSQ-CAF CM and in A549 cells treated with ApoA-*h*CAF CM, respectively (Fig. 3b and Fig. S3b). Notably, p21 staining colocalized with nuclear phosphorylated STAT1 in these cells.

To confirm the functional involvement of STAT1 activation in the antiproliferative and pro-apoptotic activities, 344SQ or A549 cells were transfected with STAT1-specific siRNA or pretreated with the pharmacologic inhibitor fludarabine (0.5 μM) before CM treatment. STAT1 knockdown attenuated the antiproliferative and pro-apoptotic effects of ApoSQ-CAF CM or ApoA-CAF CM in 344SQ and A549 cells, respectively (Fig. 3c–h and Fig. S3a–f). Similarly, fludarabine reversed these effects in 344SQ (Fig. S4a–e) and A549 cells (Fig. S4f–j). Notably, ApoSQ-CAF CM treatment of STAT1-overexpressing 344SQ cells further reduced cell viability (Fig. 3i, j), mRNA and protein expression levels of Ki67 and PCNA (Fig. 3k, l), and colony formation (Fig. 3m), and enhanced apoptotic activity compared to mock-transfected 344SQ cells treated with ApoSQ-CAF CM (Fig. 3n). These findings collectively indicate that the antiproliferative and pro-apoptotic effects were mediated via STAT1 signaling pathways.

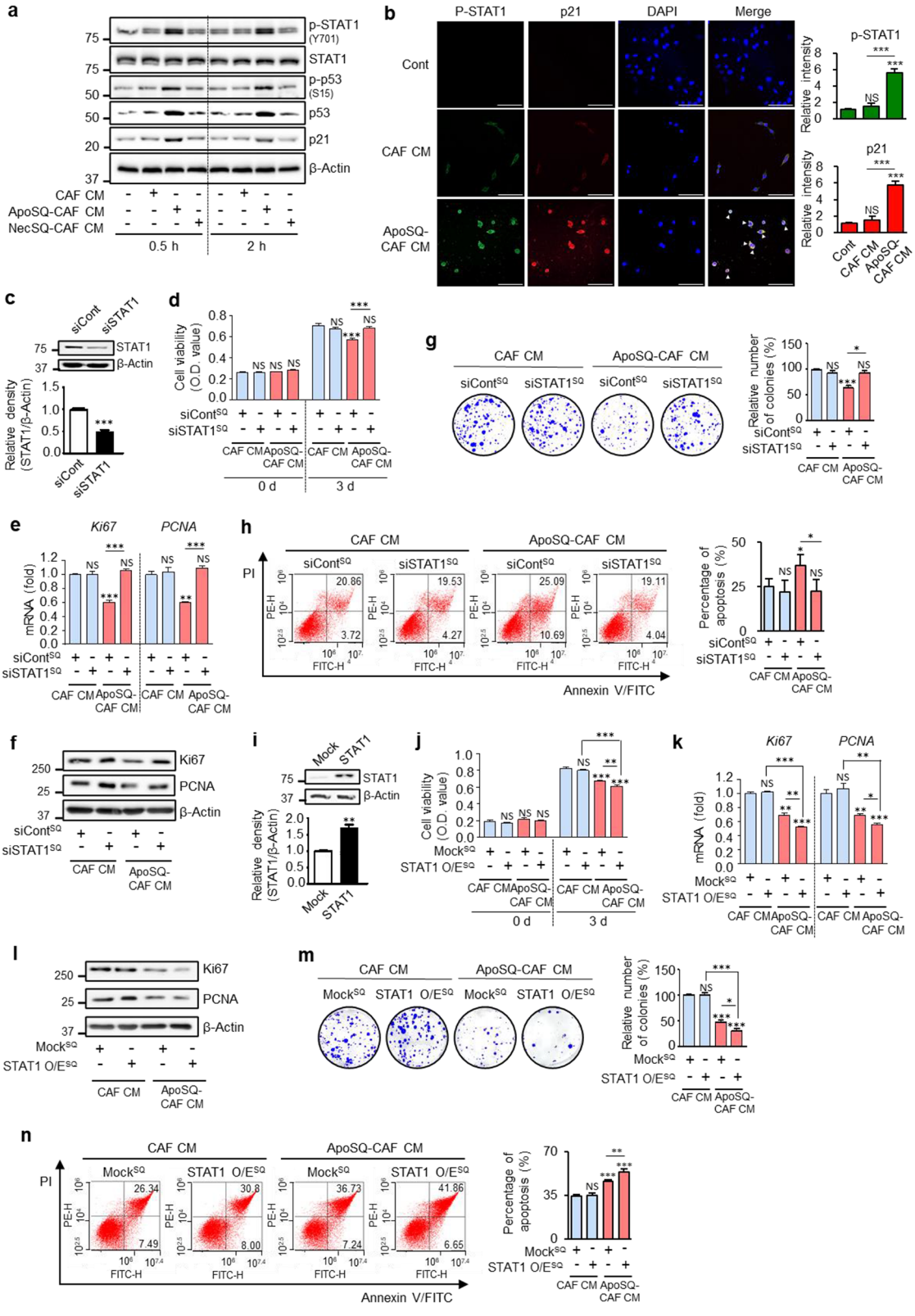

Fig. 3 (See legend on next page.)

(See figure on previous page.)

Fig. 3 STAT1 signaling is required for the antiproliferative and pro-apoptotic effects in 344SQ dells. (**a**) Immunoblot analysis of the indicated proteins in 344SQ cells treated with CAF CM, ApoSQ-CAF CM, or NecSQ-CAF CM for 0.5 and 2 h. (**b**) Immunofluorescence staining for phosphorylated STAT1 and p21 (*Left*) and quantification (*right*) in 344SQ cells for 2 h after treatment with CAF CM or ApoSQ-CAF CM. The imaging medium was VECTASHIELD fluorescence mounting medium containing DAPI. Original magnification: ×200. Scale bars = 20 μm. (**c**) Immunoblot analysis of STAT1 in 344SQ cells transfected with control or STAT1 siRNA (*upper*). (**i**) Immunoblot analysis of STAT1 in 344SQ cells transfected with control vector (mock) or the STAT1 plasmid (STAT1 O/E) for 24 h (*upper*). (**c**, **i**) Densitometric analysis of the relative STAT1 abundance (*lower*). (**d**, **j**) Cell viability assay of 344SQ cells. (**e**, **k**) qRT-PCR analysis of Ki67 and PCNA in 344SQ samples. (**f**, **l**) Immunoblot analysis of the indicated proteins in 344SQ cell lysates. (**g**, **m**) Representative images of colonies (*Left*) and quantitation of colony number formed by 344SQ cells. (**h**, **n**) *Left*: Flow cytometry analysis after Annexin V−FICT/PI dual staining was employed to evaluate the cell apoptosis of 344SQ cells. *Right*: Apoptotic cells were quantified as the sum of the percentages of early and late stages of apoptosis. (**d-h**) 344SQ cells were transfected with control or STAT1 siRNA before treatment with CM. (**j-n**) 344SQ cells were transfected with control vector or the STAT1 plasmid before treatment with CM. CAF CM or ApoSQ-CAF CM was treated to 344SQ cells for 3 (**d**-**f**, **h**, **j-l**, **n**) or 8 days (**g**, **m**). NS, not significant; $^{*}P < 0.05$, $^{**}P < 0.01$, $^{***}P < 0.001$, two-tailed Student's *t* test. Data are from one experiment representative of three independent experiments with similar results (**a**, **f**, **l**; **b**, **g**, **h**, **m**, and ***nleft***; **c** and ***iupper***) or from three independent experiments (mean ± standard error: **b**, **g**, **h**, **m**, and ***nright***; **c** and ***ilower***; **d**, **e**, **j**, **k**)

NOTCH1-dependent WISP-1 secretion from CAFs significantly contributes to the antiproliferative and pro-apoptotic effects

In our previous research, we elucidated that WISP-1 was secreted from CAFs exposed to ApoSQ via Notch1 signaling, leading to the inhibition of lung cancer cell migration and invasion [12]. In line with our prior discovery [12], WISP-1 secretion from CAFs and *h*CAFs was elevated upon exposure to ApoA, apoptotic HCT116 (ApoH), or apoptotic LoVo (ApoL), reaching levels akin to those induced by ApoSQ exposure (Supplementary Fig. S5a). Moreover, WISP-1 secretion from CAFs and *h*CAFs remained low levels in the absence of exposure to apoptotic cancer cells or when exposed to NecA, necrotic HCT116 (NecH), or necrotic LoVo (NecL). To explore whether the Notch1–WISP-1 pathway in CAFs also influences antiproliferative and pro-apoptotic effects in lung cancer cells, we conducted further investigations.

Silencing Notch1 in CAFs using specific siRNAs before ApoSQ exposure (Fig. 4a) reversed the antiproliferative and pro-apoptotic effects in 344SQ cells. This reversal was characterized by restored cell viability, increased expression of Ki-67 and PCNA mRNA and proteins, enhanced colony formation, and a simultaneous decrease in apoptosis induced by ApoSQ-CAF CM (Fig. 4b-f). Similarly, pretreatment of CAFs with a Notch1-signaling inhibitor, γ-secretase inhibitor LY3039478 (10 μM), before ApoSQ or ApoA exposure, also counteracted these effects induced by ApoSQ-CAF CM (Fig. S5b-f) and ApoA-CAF CM, respectively (Fig. S5g-k).

Furthermore, WISP-1 knockdown in CAFs by transfection with WISP-1-specific siRNA before exposure to ApoSQ reversed almost all of these antiproliferative and pro-apoptotic effects induced by ApoSQ-CAF CM (Fig. 4g-l). In addition, treatment with ApoSQ-CAF CM and ApoA-CAF CM in the presence of neutralizing anti-WISP-1 antibodies reversed these effects in 344SQ (Fig. S6a-e) and A549 cells (Fig. S6f-j). These results closely resembled the outcomes observed with Notch1 inhibition. To confirm the paracrine role of WISP-1 in inducing antiproliferative and pro-apoptotic effects, lung cancer cells were treated with mouse recombinant WISP-1 (rWISP-1, 20–100 ng/ml). As anticipated, rWISP-1 dose dependently inhibited cellular viability, reduced Ki67 and PCNA mRNA and protein expression, and suppressed colony formation both 344SQ (Fig. 5a–d) and A549 cells (Fig. S7a-d). Flow cytometric analysis and TUNEL assays revealed that rWSIP-1 promoted apoptosis of lung cancer cells in a dose-dependent manner over 1–3 days and 2 days, respectively, in 344SQ (Fig. 5e, f) and A549 cells (Fig. S7e, f). Furthermore, rWISP-1 increased pro-apoptotic markers like Bax, cleaved caspase-3, and cleaved PARP, whereas the anti-apoptotic proteins Bcl-2, Mcl-1, or Bcl-xL decreased in a dose-dependent manner in both 344SQ (Fig. 5g) and A549 cells (Fig. S7g). These results strongly support WISP-1 secretion from CAFs exposed to apoptotic lung cancer cells mediating the observed antiproliferative and pro-apoptotic effects.

WISP-1 signaling via the αvβ3-STAT1 pathway inhibits proliferation and promotes apoptosis in lung cancer cells

WISP-1 functions by binding to integrins, essential cell surface receptors [24, 25]. In a previous study, we utilized blocking antibodies against integrin αv, α5, β1, β3, or β5, and identified the integrin αv and β3 involvement in the inhibitory effects of WISP-1 on TGF-β1-induced migration and invasion of lung cancer cells [12]. Similarly, pretreatment with anti-integrin αv or β3 antibodies substantially reversed the antiproliferative and pro-apoptotic effects of rWISP-1 (50 ng/ml) in 344SQ (Fig. 6a–e) and A549 cells (Fig. S8a–e). However, anti-integrin α5 or β5 antibodies did not exhibit the reversive effect on proliferation of 344SQ cells (Fig. S8f). Moreover, anti-integrin αv or β3 antibodies reversed the enhanced STAT1 activity and downstream molecule expression, including increased p53 phosphorylation and p53 and p21 expression induced by rWISP-1 in 344SQ (Fig. 6f) and A549 cells (Fig. S8g). Similarly, knockdown of STAT1 reversed the antiproliferative and pro-apoptotic effects, along with the enhanced p53 phosphorylation and p53 and p21 expression induced by rWISP-1 in 344SQ (Fig. 6g–l) and A549 cells (Fig. S8h–m), indicating the mediating role of STAT1 signaling in the antiproliferative and

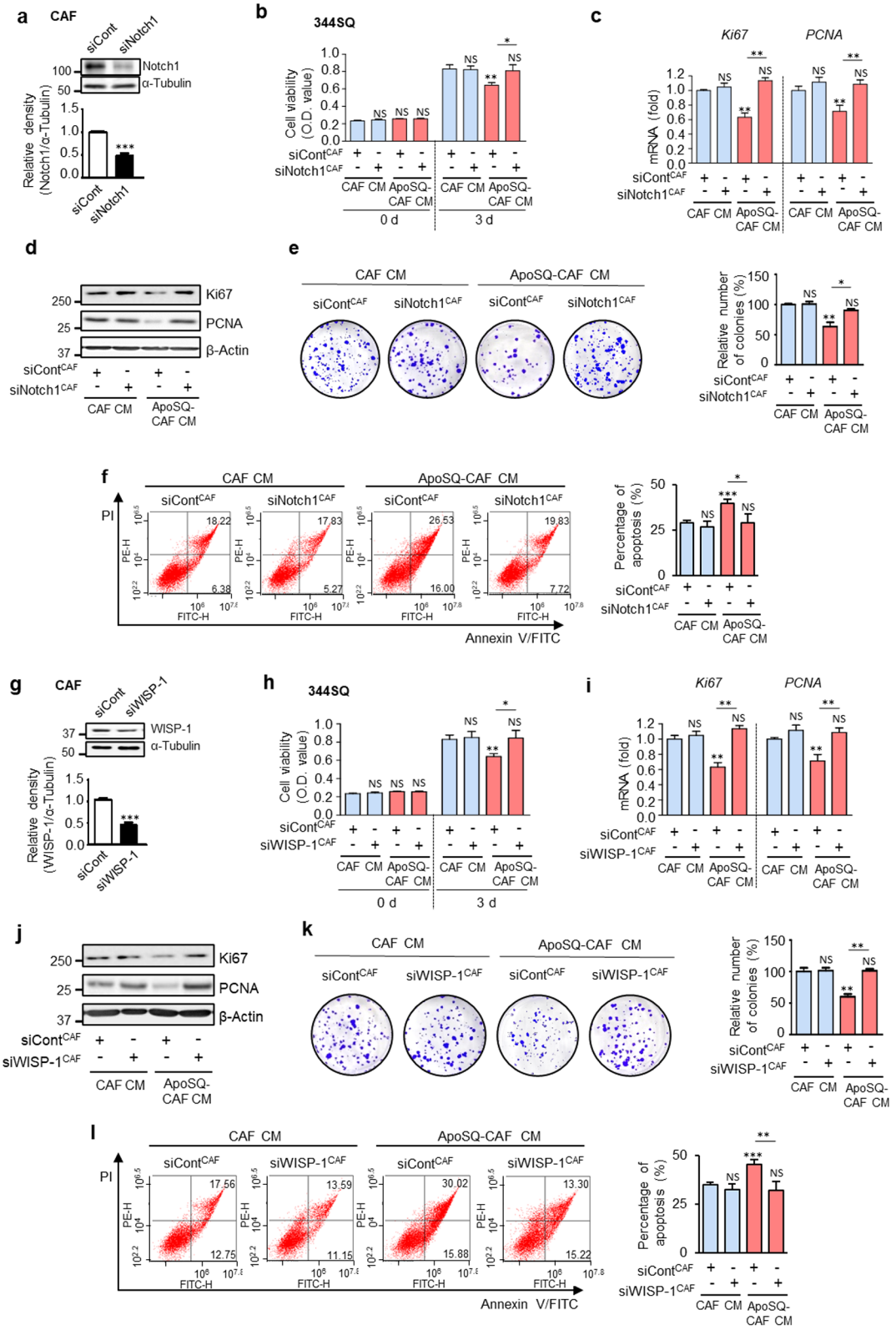

Fig. 4 (See legend on next page.)

(See figure on previous page.)

Fig. 4 Disrupting Notch1 and WISP-1 in CAFs reverses the antiproliferative and pro-apoptotic effects of ApoSQ-CAF CM in 344SQ cells. (**a**, **g**) Immunoblot analysis of Notch1 (**a**) or WISP-1 (**g**) in CAFs transfected with control, Notch1, or WISP-1 siRNA (*upper*). Densitometric analysis of the relative Notch1 or WISP-1 abundance (*lower*). (**b**, **h**) Cell viability assay of 344SQ cells. (**c**, **i**) qRT-PCR analysis of Ki67 and PCNA in 344SQ samples. (**d**, **j**) Immunoblot analysis of Ki67 and PCNA in 344SQ lysates. (**e**, **k**) *Left*: Representative images of colonies formed by 344SQ cells. *Right*: Quantitation of colony number formed by these cancer cells. (**f**, **l**) *Left*: Flow cytometry analysis after Annexin V – FICT/PI dual staining was employed to evaluate the apoptosis of 344SQ cells. *Right*: Apoptotic cells were quantified as the sum of the percentages of early and late stages of apoptosis. (**b**-**f**) CAFs were transfected with control or Notch1 siRNA before exposure to apoptotic 344SQ cells (ApoSQ) for 20 h. (**h**-**l**) CAFs were transfected with control or WISP-1 siRNA before exposure to ApoSQ for 20 h. CM was added to 344SQ cells for 3 (**b**-**d**, **f**, **h**-**j**, **l**) or 8 days (**e**, **k**). NS, not significant; $^{*}P < 0.05$, $^{**}P < 0.01$, $^{***}P < 0.001$, two-tailed Student's *t* test. Data are from one experiment representative of three independent experiments with similar results (**a** and ***gupper***; **d**, **j**; **e**, **f**, **k**, and ***lleft***) or from three independent experiments (mean ± standard error: **a** and ***gbelow***; **b**, **c**, **h**, **i**; **e**, **f**, **k**, and ***lright***)

pro-apoptotic effects of rWISP-1. To verify the role of the integrin αvβ3 receptor in signaling pathways that mediate antiproliferative and pro-apoptotic effects in lung cancer cells in response to WISP-1, we silenced integrin αv or β3 using specific siRNAs. The knockdown of integrin αv or β3 (Fig. S9a, e) substantially reversed the antiproliferative and pro-apoptotic effects induced by rWISP-1 (50 ng/ml) in both 344SQ (Fig. S9b, c) and A549 cells (Fig. S9f, g). Moreover, siRNAs targeting αv or β3 markedly reduced STAT1 phosphorylation in these lung cancer cells (Fig. S9d, h). Taken together, these results validate WISP-1 signals through the integrin αvβ3-STAT1 pathway to inhibit proliferation and promote apoptosis in lung cancer cells. To further confirm that integrin αvβ3 is a receptor for WISP-1, we performed CoIP assay to assess their interaction. Using an anti-WISP-1 antibody, we successfully pulled down WISP-1, which was found to co-precipitate with integrin αv and β3 in 344SQ (Fig. 6m) and A549 cells (Fig. S9i). Collectively, these data validate that integrin αvβ3 acts as the receptor for WISP-1 in paracrine signaling within lung cancer cells.

To verify the clinical significance between CCN4 and STAT1 in lung adenocarcinoma (LUAD) patients, we conducted comprehensive bioinformatic analyses. A single-cell RNA sequencing dataset comprising 19 LUAD studies and involving 309 patients [26] revealed that *CCN4* expression is minimal in epithelial cells but highly expressed in bronchial fibroblasts characterized by *FAP* expression, whereas *STAT1* is predominantly expressed in malignant cells (Fig. S10). The number of extracted cells is described in Table S4. Bulk RNA-sequencing data from the CPTAC (Clinical Proteomic Tumor Analysis Consortium) study, involving 110 patients, demonstrated a negative correlation between *CCN4* expression levels and tumor purity and a positive correlation with the stromal score, indicating that *CCN4* expression predominantly occurs in non-tumor stromal cells (Table S5). Furthermore, significant quantitative correlations between *CCN4* and *STAT1* expression were observed in both the CPTAC-LUAD and the TCGA (The Cancer Genome Atlas; $n = 510$) studies. In addition, CPTAC phosphoproteome data revealed that the phospho-protein abundance of STAT1-Ser727, a site phosphorylated following STAT1-Tyr701 phosphorylation [27], is significantly positively correlated with *CCN4* expression. Thus, these findings suggest that WISP-1 (CCN4) secreted from CAFs may stimulate STAT1 activation in malignant cells in clinical settings.

WISP-1 activates STAT1 signaling to drive the anti-tumor growth effect of ApoSQ-CAF CM *in vivo*

To explore the in vivo impact of WISP-1 signaling on tumor growth inhibition through paracrine mechanisms, we pre-incubated CM with either a neutralizing antibody against WISP-1 or an IgG isotype control antibody for 2 h before injection into mice (Fig. 7a). Notably, the observed reduction in tumor volume over time with undiluted ApoSQ-CAF CM injection was abrogated when WISP-1-immunodepleted ApoSQ-CAF CM was administered (Fig. 7b).

Immunofluorescent staining of serial sections of primary tumor tissue revealed a decrease in Ki67-positive proliferative tumor cells (Fig. 7c, d) and an increase in apoptosis of tumor cells, as marked by cleaved caspase-3 in $CD326^{+}$ tumor cells (Fig. 7e, f), following ApoSQ-CAF CM injection. However, these effects were reversed with the administration of WISP-1-immunodepleted ApoSQ-CAF CM. Notably, CM containing the IgG isotype control exhibited effects similar to those of ApoSQ-CAF CM.

Consistent with our in vitro findings, elevated levels of phosphorylated STAT1, phosphorylated p53, p53, p21, and cleaved caspase-3 protein expression were observed in $CD326^{+}$ tumor cells isolated from primary tumors in the ApoSQ-CAF CM group (Fig. 7g). Moreover, a decrease in Bcl-2 and Ki67 expression was evident in the same group. However, these changes were absent in the WISP-1-immunodepleted ApoSQ-CAF CM group.

Furthermore, immunohistochemical analysis confirmed alterations in the levels of phosphorylated STAT1 in $CD326^{+}$ tumor cells (Fig. 7h, i). Additionally, Pearson's correlation coefficient revealed a negative correlation between WISP-1 levels in the CM (Fig. 7j) or the intensity of phosphorylated STAT1 staining (Fig. 7k) in $CD326^{+}$ tumor cells of primary tumor tissue and tumor volume, as well as Ki67 staining levels, and showed a positive correlation with cleaved caspase-3 staining levels in $CD326^{+}$ tumor cells.

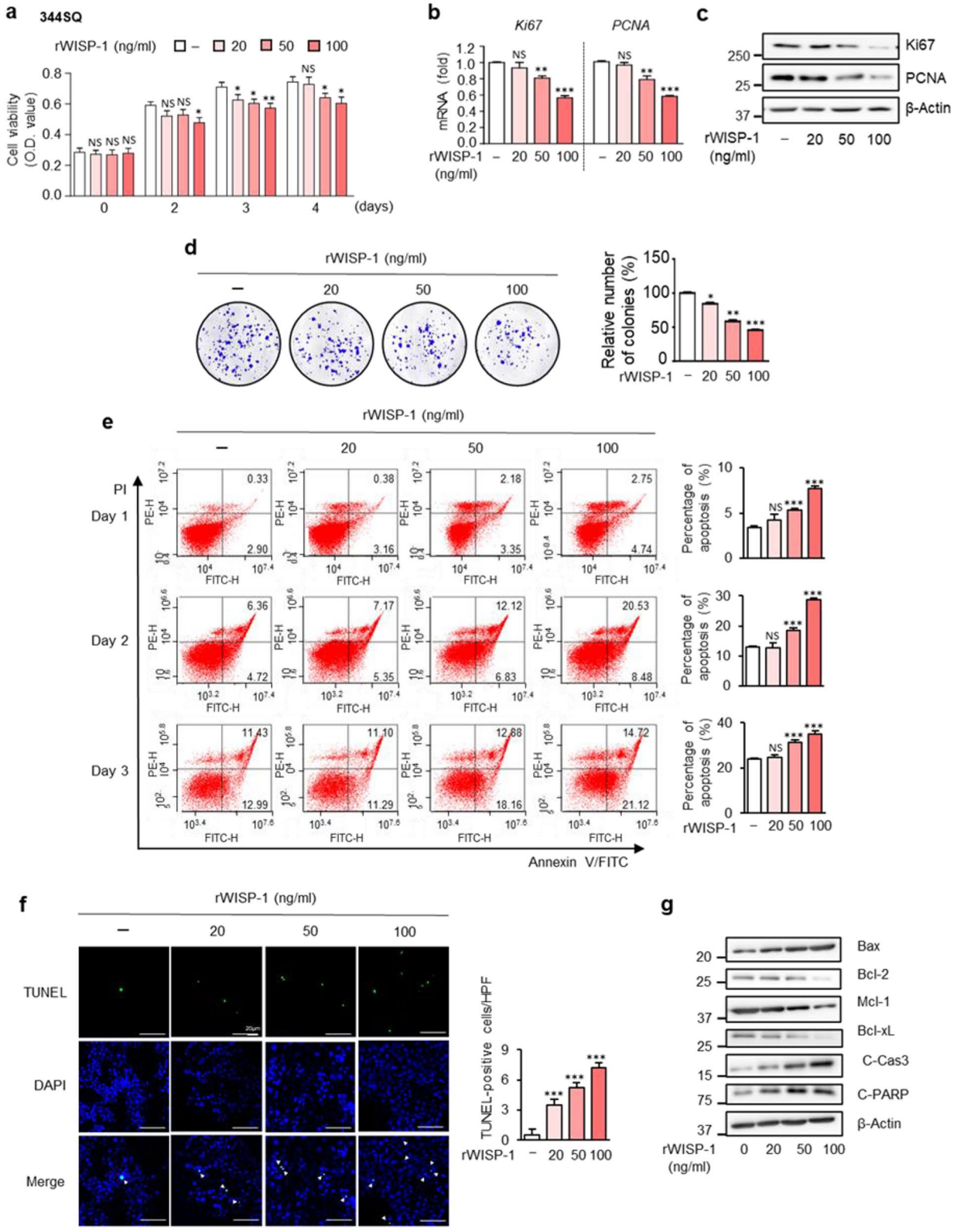

Fig. 5 (See legend on next page.)

(See figure on previous page.)

Fig. 5 Recombinant WISP-1 suppresses proliferation and promotes apoptosis in 344SQ cells. (**a**) Cell viability assay of 344SQ cells. (**b**) qRT-PCR analysis of Ki67 and PCNA in 344SQ samples. (**c**) Immunoblot analysis of Ki67 and PCNA in 344SQ cell lysates. (**d**) *Left*: Representative images of colonies formed by 344SQ cells. *Right*: Quantitation of colony number formed by 344SQ cells. (**e**) *Left*: Flow cytometry analysis after Annexin V – FICT/PI dual staining was employed to evaluate the cell apoptosis of 344SQ cells. *Right*: Apoptotic cells were quantified as the sum of the percentages of early and late stages of apoptosis. (**f**) *Left*: Representative images of apoptosis in 344SQ cells by TUNEL assay (original magnification: x200). Nuclei were observed by DAPI staining. Scale bar = 20 μm. *Right*: Quantitation of the number of TUNEL – positive cells (number/HPF) in the different groups. (**g**) *Left*: Immunoblot analysis of Bax, Bcl-2, Mcl-1, Bcl-kL, cleaved caspase-3, cleaved PARP, and β-actin in 344SQ lysates. 344SQ cells were treated with recombinant WISP-1 (rWISP-1; 20, 50, and 100 ng/ml) for 2–4 (**a**), 3 (**b**, **c**, **g**), 8 (**d**), 1–3 (**e**), or 2 days (**f**). NS, not significant; $^{*}P < 0.05$, $^{**}P < 0.01$, $^{***}P < 0.001$, two-tailed Student's *t* test. Data are from one experiment representative of three independent experiments with similar results (**c**, **g**; **d-*fleft***) or from three independent experiments (mean ± standard error: **a**, **b; d-*fright***)

In our previous study, we demonstrated that intratumoral injection of rWISP-1 reduced both the weight and volume of the primary tumor, as well as the metastasis rate, compared to the control group [12]. In the current study, we found through immunofluorescent staining assay in primary tumor tissue that rWISP-1 injection (12.5 and 25 μg/kg) (Fig. 8a) resulted in a decrease in Ki67-positive proliferative tumor cells (Fig. 8b, c), an increase in apoptosis of tumor cells (Fig. 8d, e), and enhanced phosphorylated STAT1 staining in tumor cells (Fig. 8f, g). Moreover, rWISP-1 increased the levels of phosphorylated STAT1, phosphorylated p53, p53, p21, and cleaved caspase-3 protein expression, while decreasing Bcl-2 and Ki67 expression in $CD326^{+}$ tumor cells isolated from primary tumors (Fig. 8h).

We further examined the tumor-suppressive role of STAT1 in rWISP-1-treated mice using fludarabine. Pretreatment with 10 mg/kg fludarabine one hour before administering rWISP-1 (25 μg/kg) did not affect the body weight (Fig. 9a, b). However, fludarabine abolished the anti-tumor effects of rWISP-1, reversing the reductions in tumor weight and volume, as well as decreases in the number of tumor nodules on the lung surface and the metastatic rate (Fig. 9c-h). Immunofluorescent staining further demonstrated that fludarabine treatment counteracted the rWISP-1-induced reductions in Ki67-positive tumor cells and phosphorylated STAT1 levels, as well as the increase in tumor cell apoptosis (Fig. 9i-n). These findings collectively indicate that the anti-tumor effects of ApoSQ-CAF CM are mediated through the WISP-1-STAT1 signaling pathway, with rWISP-1 effectively replicating the in vivo anti-tumor effects of ApoSQ-CAF CM.

Discussion

The present study contributes to our advancing knowledge of the important roles of apoptotic cancer cells within the TME which could reprogram nonprofessional phagocytes CAFs, consequently enhancing antiproliferative and pro-apoptotic effects in lung cancer cells through WISP-1 production. We specifically identified the WISP-1–integrin αvβ3–STAT1 signaling pathways as crucial in mediating the crosstalk between CAFs and lung cancer cells, presenting promising targets for therapeutic intervention. Our findings extend beyond lung cancer cells, suggesting a broader impact on tumor progression. Notably, apoptotic cancer cell-exposed CAF CM exhibits cross-activity with various types of cancer cells across different species, including mice and humans. Although apoptotic bodies, vesicles, and soluble factors released from apoptotic tumor cells influence tumor progression [28], our experimental conditions excluded direct effects of apoptotic cell–derived CM on cancer cell proliferation, as the CM from apoptotic lung cancer cells and colon cancer cell lines alone did not affect cancer cell proliferation. By using a transwell assay to culture CAFs with apoptotic cancer cells without direct contact, it was clarified that direct cell-cell contact is necessary for the observed suppression.

Flow cytometry analysis after Annexin V-FITC/PI staining and TUNEL assays revealed that treatment with ApoSQ-CAF CM or ApoA-CAF CM promoted apoptosis in lung cancer cells. Moreover, we conducted a detailed examination of the expression signature of apoptosis-related proteins, offering mechanistic insights into the apoptotic pathway. Our study highlights the pivotal role of the mitochondrial pathway of apoptosis, where the Bcl-2 family of proteins facilitates the release of pro-apoptotic factors from the mitochondrial inner membrane space [29]. The balance between anti-apoptotic proteins like Bcl-2 or Mcl1 and the pro-apoptotic protein Bax critically influences cell susceptibility to apoptosis by regulating cytochrome c and initiating downstream apoptotic events [30, 31]. Specifically, cytochrome c release activates caspases, a family of proteases pivotal in apoptosis, including the executioner caspase-3 [32], which is crucial to apoptosis initiation.

In our study, treatment with ApoSQ-CAF CM or ApoA-CAF CM reduced the ratio of Bcl-2, Mcl-1, or Bcl-xL to Bax in 344SQ and A549 cells. This reduction in the ratio of anti-apoptotic to pro-apoptotic proteins activated caspases, notably cleaved caspase-3, leading to PARP cleavage, a hallmark of apoptotic cell death. Additionally, we observed increased levels of cleaved caspase-3 and cleaved PARP. These results highlight the pro-apoptotic activity of CM from CAFs exposed to apoptotic lung cancer cells, influencing cell fate and inhibiting cancer cell proliferation.

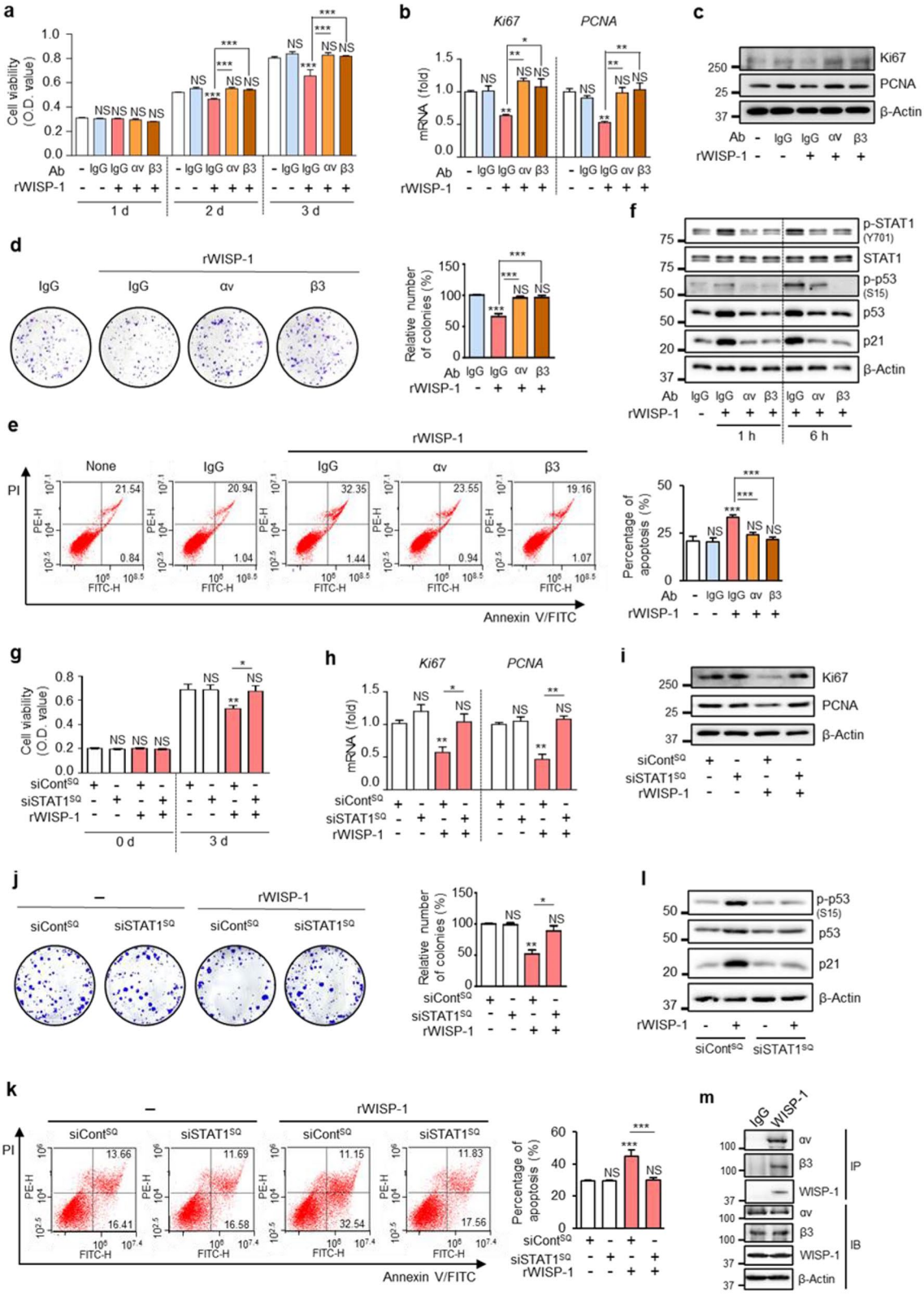

Fig. 6 (See legend on next page.)

(See figure on previous page.)

Fig. 6 WISP-1 acts through integrin αvβ3 to activate STAT1 in 344SQ cells. (**a**, **g**) Cell viability assay of 344SQ cells. (**b**, **h**) qRT-PCR analysis of Ki67 and PCNA in 344SQ samples. (**c**, **f**, **i**, **l**) Immunoblot analysis of the indicated proteins in 344SQ lysates. (**d**, **j**) Representative images of colonies (*Left*) and quantitation of colony number formed by 344SQ cells (*right*). (**e**, **k**) *Left*: Flow cytometry analysis after Annexin V – FICT/PI dual staining was employed to evaluate the apoptosis of 344SQ cells. *Right*: Apoptotic cells were quantified as the sum of the percentages of early and late stages of apoptosis. (**a-f**) 344SQ cells were pretreated with an anti-integrin blocking antibody (3 μg/ml; anti-integrin αv or β3) or corresponding IgG isotype control for 30 min before treatment with 50 ng/ml rWISP-1 for the indicated time, 3 (**b**, **c**, **e**) or 8 days (**d**). (**g**-**l**) 344SQ cells were transfected with control or STAT1 siRNA before treatment with 50 ng/ml rWISP-1 for 1 h (**l**), 3 (**g**, **h**, **i**, **k**), or 8 days (**j**). (**i**) CoIP assays of protein interaction in 344SQ cells. Cell lysates were immunoprecipitated (IP) with anti-WISP-1 and then immunoblotted with anti-integrin αv and anti-integrin β3 antibodies. NS: not significant; $^{*}P < 0.05$, $^{**}P < 0.01$, $^{***}P < 0.001$, two-tailed Student's *t*-test. The data are from one experiment representative of three independent experiments with similar results (**c**, **f**, **i**, **l**, **m**; **d**, **e**, **j**, and **k***left*) or from three independent experiments (mean ± standard error: **a**, **b**, **g**, **h**; **d**, **e**, **j**, and **k***right*)

STAT1 exhibits both pro-apoptotic and antiproliferative activities in tumor cells [33]. Zhang et al. [34] further supported this notion by demonstrating its tumor-suppressive effects in esophageal squamous carcinoma, where it modulates key regulators of apoptosis and cell cycle progression, including Bcl-2, Bcl-xL, survivin, cyclin D1, and p21. STAT1-deficient mice exhibit increased susceptibility to tumor development compared to those with wild-type STAT1 [20, 21]. In our study, ApoSQ-CAF CM or ApoA-CAF CM treatment activated the STAT1 signaling pathway, inhibiting proliferation and promoting apoptosis in lung cancer cells. STAT1 knockdown and its inhibitor fludarabine reversed these effects, whereas STAT1 overexpression intensified the antiproliferative and pro-apoptotic effects of ApoSQ-CAF CM.

In our previous study, cytokine array analysis revealed that WISP-1 is the most highly increased in ApoSQ-CAF CM compared with CAF CM and ApoSQ CM [12]. Additionally, we identified a novel mechanism in which increased expression of the Notch ligand delta-like protein 1 on the surface of ultraviolet-irradiated apoptotic lung cancer cells activates Notch1 signaling in CAFs, leading to the upregulation of WISP-1 transcription. In the current study, inhibiting Notch1 signaling in CAFs using the pharmacological inhibitor LY3039478 or Notch1-specific siRNAs reversed the proliferation suppression and apoptosis promotion induced by ApoSQ-CAF CM and ApoA-CAF CM in 344SQ and A549 cells, respectively. Additionally, WISP-1 knockdown in CAFs or WISP-1 immunodepletion in CM attenuated the antiproliferative and pro-apoptotic effects of these CM. Direct treatment of these lung cancer cells with 20–100 ng/ml rWISP-1 dose dependently inhibited cell proliferation and promoted apoptosis. These data confirm that WISP-1, secreted from CAFs upon exposure to apoptotic lung cancer cells, exerts a paracrine effect on neighboring lung cancer cells. Similarly, overexpression of Notch1 signaling in stromal fibroblasts has been shown to suppress cell growth via upregulation of WISP-1 in melanoma [35]. In lung cancer cells, WISP-1 overexpression inhibits its invasion, migration and metastasis via suppression of Rac activity [36]. However, conflicting reports suggest an oncogenic role for WISP-1 in glioblastoma and melanoma [37, 38]. Expression of WISP-1 correlates with clinical features of lung cancer [39]. This discrepancy among studies may be attributed to differences in cancer type and stage, variations in WISP-1 concentration within the TME, and the specific cellular context. Therefore, further comprehensive investigations are needed to elucidate the detailed functions and molecular mechanisms of WISP-1 in either suppressing or promoting lung cancer progression.

Several studies have demonstrated that WISP-1 influences cellular functions by binding to cell surface receptors known as integrins [24, 25]. Integrins, composed of various combinations of α and β subunits, regulate a wide array of cellular responses in a cell-specific manner [40, 41]. In our prior study, we illustrated that WISP-1 signals through integrin αvβ3 in 344SQ cells and αvβ5 in CAFs, effectively suppressing TGF-β1-induced migration and invasion [12]. In vitro and in vivo murine melanoma models offer conflicting insights into the effects of the integrin αvβ3 antagonist cilengitide. Although cilengitide decreases tumor cell proliferation, migration, and neoangiogenesis [42], primary tumor growth is unexpectedly enhanced in integrin $\beta3^{-/-}$ mice due to enhanced pathological angiogenesis [43]. Despite promising preclinical data, integrin β3 antagonists have not shown improved outcomes in several cancer types in clinical trials [44–46]. The integrin αvβ3-JAK2-STAT1 pathway is implicated in upregulating apoptosis in A549 cells [47]. In this study, using blocking antibodies against integrin αv or β3 and specific siRNA targeting αv or β3, we found that exogenous rWISP-1 activates STAT1 signaling pathways via integrin αvβ3. This activation leads to antiproliferative and pro-apoptotic effects in 344SQ and A549 cells. CoIP assays confirmed that integrin αvβ3 is a receptor for WISP-1 in 344SQ and A549 cells. These findings collectively suggest that Notch1-dependent WISP-1 secretion from CAFs, triggered by apoptotic lung cancer cells, plays an essential role in suppressing proliferation and promoting apoptosis in lung cancer cells through integrin αvβ3-STAT1 signaling pathways.

Single-cell RNA sequencing data from LUAD patients reveals that *CCN4* is highly expressed in *FAP* + fibroblasts, while *STAT1* is mainly expressed in malignant cells, suggesting a paracrine signaling mechanism. This observation is further supported by large-scale

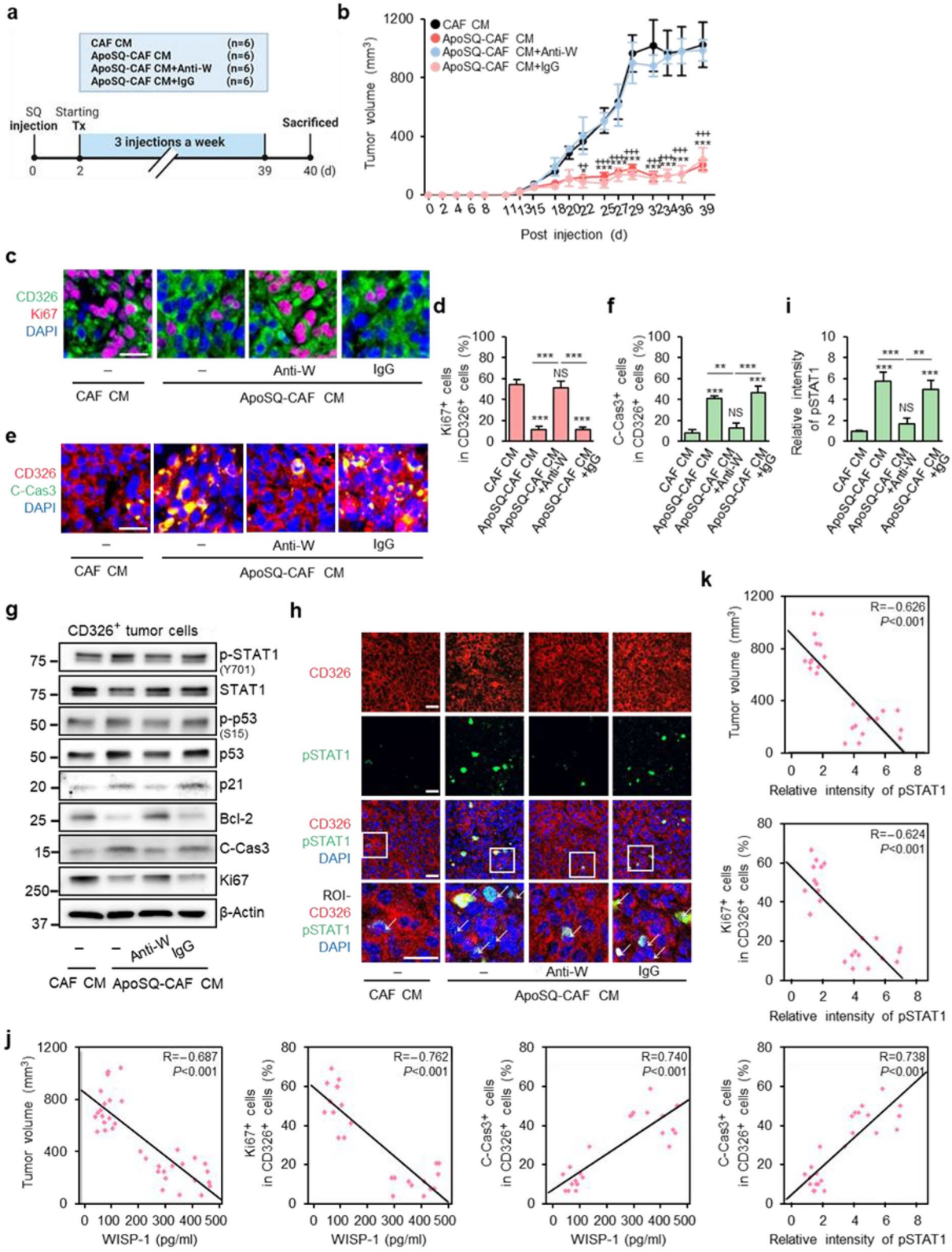

Fig. 7 (See legend on next page.)

(See figure on previous page.)

Fig. 7 Injection of ApoSQ-CAF CM suppresses tumor growth via WISP-1/STAT1 signaling in mice. (**a**) Schematic of experimental design and groups. CAF CM, ApoSQ-CAF CM, ApoSQ-CAF CM + anti-WISP-1, or ApoSQ-CAF CM + IgG was intratumorally injected three times a week for 6 weeks starting 2 days after subcutaneous injection of 344SQ cells into syngeneic (129/Sv) mice ($n = 6$ mice per group). Mice were necropsied 6 weeks later. (**b**) Tumor volume was measured at the indicated days. $^{*}P < 0.05$, $^{***}P < 0.001$ for ApoSQ-CAF CM vs. CAF CM; $^{++}P < 0.01$, $^{+++}P < 0.001$ for ApoSQ-CAF CM + IgG vs. CAF CM, Analysis of variance with Tukey's post hoc test. The data are presented as the mean ± standard error of results from 6 mice per group. (**c**, **e**, **h**) Representative confocal images of primary tumor sections stained with an anti-Ki67 antibody (red; **c**), an anti-cleaved caspase-3 antibody (green; **e**), anti-phophorylated STAT1 (green; **h**), an anti-326 antibody (green or red), and DAPI (blue). ROI – Merge panels show high-magnification of regions of interest as indicated by white squares in Merge panels (**h**). Original magnification: ×40. Scale bars = 100 µm. (**d**, **f**, **i**) Quantification of Ki67^{+}, cleaved caspase-3^{+} cells, and relative fluorescence intensity of phosphorylated STAT1 staining among CD326^{+} cells. The data are represented as the means ± standard errors from three mice per group. NS, not significant; $^{**}P < 0.01$, $^{***}P < 0.001$, Analysis of variance with Tukey's post hoc test. (**g**) Immunoblot analysis of the indicated proteins in isolated CD326^{+} tumor cells. The data are from three replicates per condition, with cells pooled from three mice per replicate. The data are from one experiment representative of three independent experiments with similar results (**c**, **e**, **g**, **h**). (**j**) The Pearson's correlations between the levels of WISP-1 in CM evaluated by ELISA and tumor volume, Ki-67^{+} or cleaved caspase^{+} cells in CD326^{+} tumor cells. (**k**) The Pearson's correlations between phosphorylated STAT1 fluorescence intensity in CD326^{+} tumor cells and tumor volume, Ki-67^{+} or cleaved caspase^{+} cells in CD326^{+} tumor cells. $P < 0.001$

public high-throughput data from clinical LUAD samples, which suggest stromal expression of *CCN4*. Bioinformatic analyses identified a significant correlation between *CCN4* and *STAT1* expression, highlighting the influence of the TME on tumor behavior. Additionally, phosphoproteomic data suggest that WISP-1 secreted by CAFs may activate STAT1 in tumor cells. These findings emphasize the critical role of the TME in regulating tumor cell proliferation and apoptosis in LUAD through modulation of STAT1-related signaling pathways.

Consistent with our in vitro results, intratumoral administration of diluted ApoSQ-CAFCM (50%) weakened its inhibitory effect on tumor growth compared to undiluted CM, indicating that ApoSQ-exposed CAFs are crucial for suppressing tumor growth through paracrine signaling. qRT-PCR array analysis further revealed downregulation of genes associated with cell cycle progression and anti-apoptotic pathways in CD326^{+} tumor cells from primary tumors after ApoSQ-CAF CM injection, supporting its anti-growth effect. Additionally, our in vivo experiments confirmed WISP-1's pivotal role in ApoSQ-CAF CM-mediated tumor growth suppression as a paracrine mediator; injection of WISP-1-immunodepleted ApoSQ-CAF CM reversed the anti-tumor growth effect. Immunohistochemistry analysis of primary tumor tissue further supported the WISP-1-dependent antiproliferative and pro-apoptotic effects of ApoSQ-CAF CM by demonstrating reduced Ki67 expression and increased cleaved caspase-3 expression in CD326^{+} tumor cells. Consistent with our in vitro data, immunofluorescence analysis of primary tumor sections and Western blot analysis of isolated CD326^{+} tumor cells indicated that ApoSQ-CAF CM injection activates WISP-1-dependent STAT1 signaling, modulating the expression of STAT1 key regulators associated with apoptosis and cell cycle arrest. Similarly, intratumoral injection of rWISP-1 demonstrated the anti-tumor growth effect through activation of the STAT1 signaling pathway.

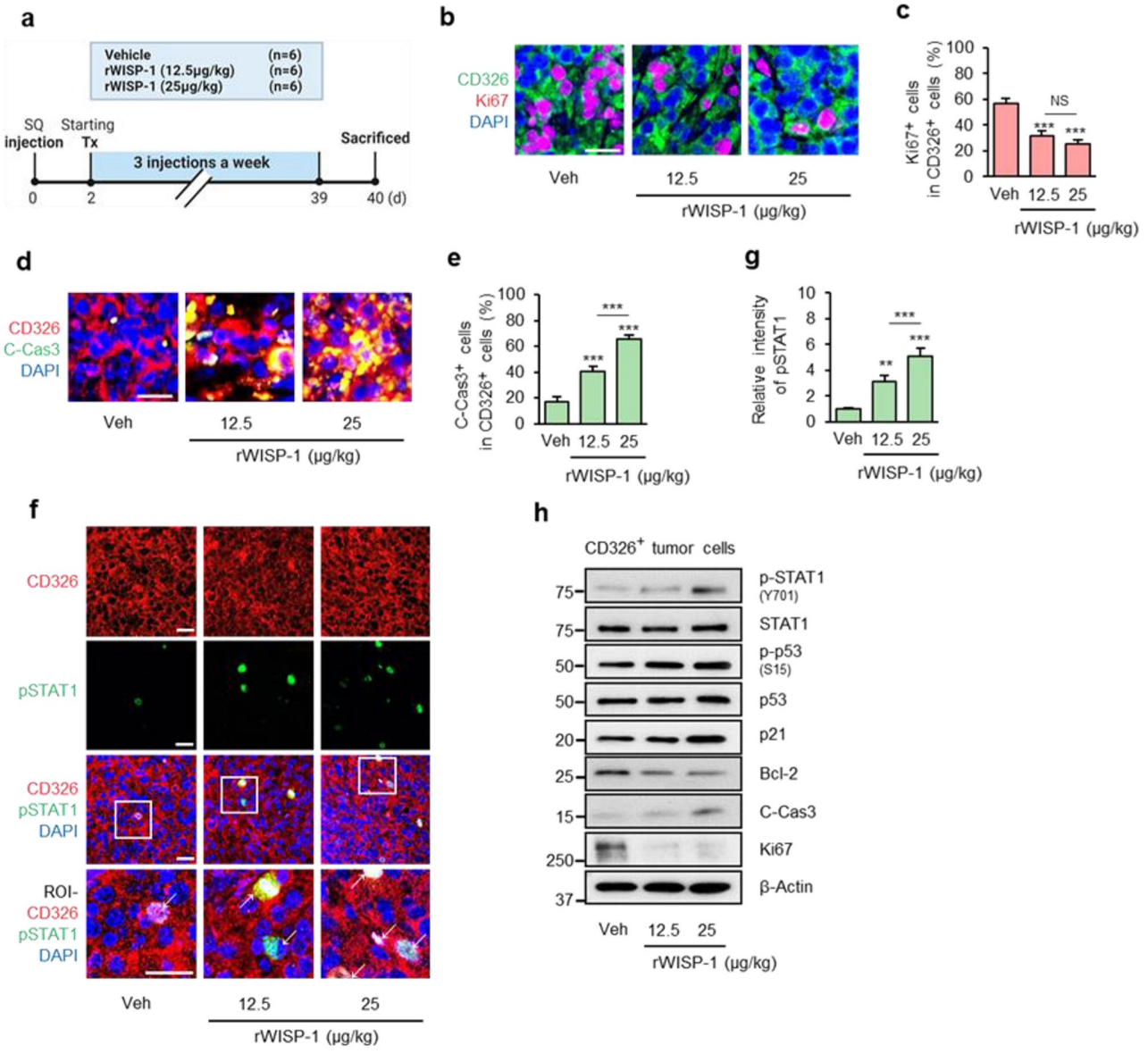

Fig. 8 Recombinant WISP-1 modulates the proliferation and apoptosis markers of tumor cells in mice. (**a**) Schematic of experimental design. Where indicated, rWISP-1 (12.5 and 25 μg/kg) was administered intratumorally three times a week for 6 weeks beginning 2 days after subcutaneous injection of 344SQ cells into syngeneic (129/Sv) mice ($n = 6$ mice per group). Mice were necropsied 6 weeks later. (**b**, **d**, **f**) Representative confocal images of primary tumor sections stained with an anti-Ki67 antibody (red; **b**), an anti-cleaved caspase-3 antibody (green; **d**), anti-phophorylated STAT1 (green; **f**), an anti-326 antibody (green or red), and DAPI (blue). ROI – Merge panels show high-magnification of regions of interest as indicated by white squares in Merge panels (**f**). Original magnification: ×40. Scale bars = 100 μm. (**c**, **e**, **g**) Quantification of $Ki67^+$, cleaved caspase-3^+ cells, and relative fluorescence intensity of phosphorylated STAT1 staining among $CD326^+$ cells. The data are represented as the means ± standard errors from three mice per group. NS, not significant; $^{**}P < 0.01$, $^{***}P < 0.001$, Analysis of variance with Tukey's post hoc test. (**h**) Immunoblot analysis of the indicated proteins in isolated $CD326^+$ tumor cells. The data are from three replicates per condition, with cells pooled from three mice per replicate. The data are from one experiment representative of three independent experiments with similar results (**b**, **d**, **f**, **h**)

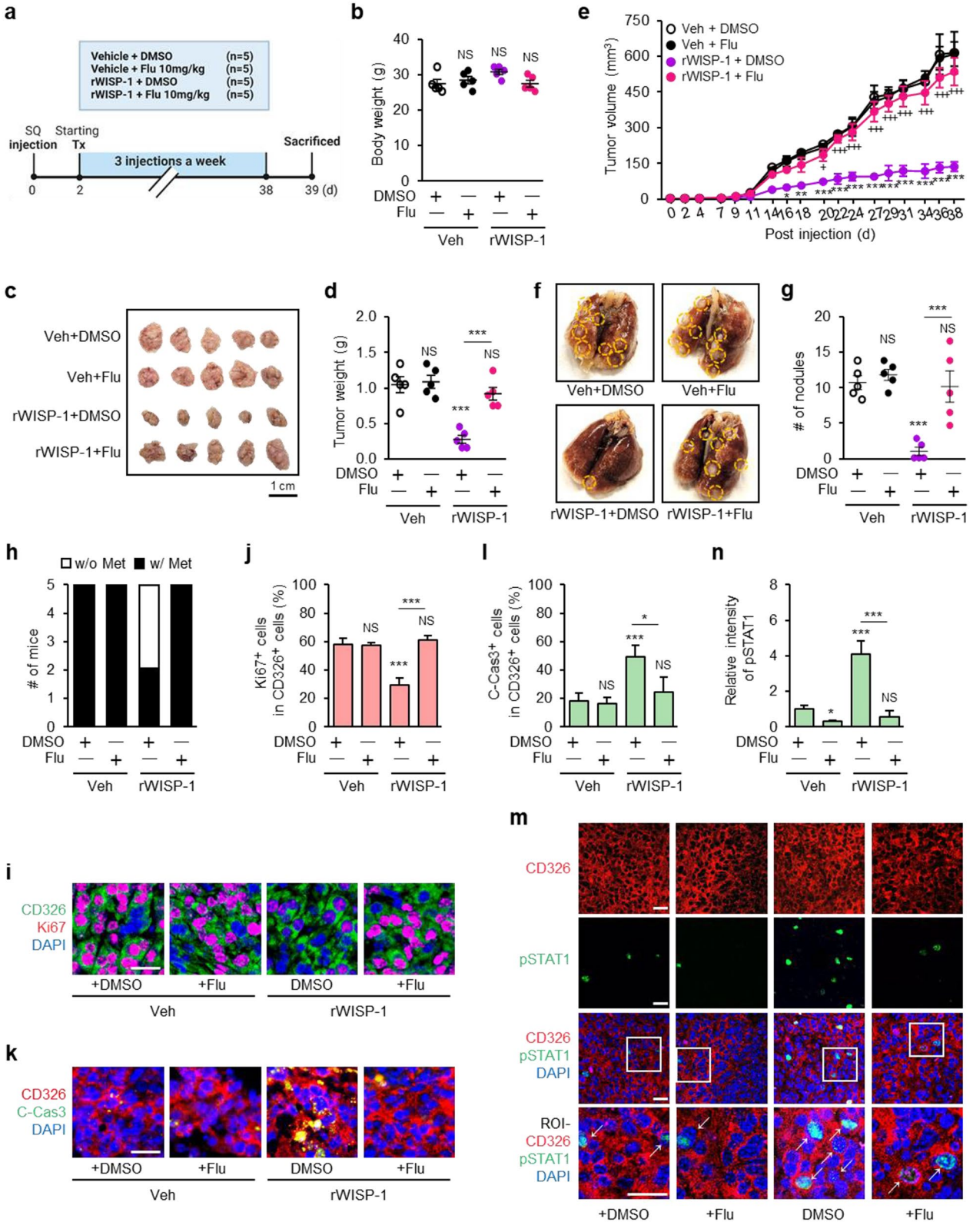

Fig. 9 (See legend on next page.)

(See figure on previous page.)

Fig. 9 WISP-1-STAT1 signaling suppresses tumor growth in mice. (**a**) Schematic of experimental design. Where indicated, fludarabine (10 mg/kg) or 5% DMSO was administrated via intraperitoneal injection 1 h prior to the intratumoral injection of rWISP-1 (25 μg/kg). The rWISP-1 injections were performed three times per week for 6 weeks, starting 2 days after the subcutaneous injection of 344SQ cells into syngeneic (129/Sv) mice ($n = 5$ mice per group). Mice were necropsied 6 weeks later. Scatter plots of body weight (**b**), primary tumor weight (**d**), and numbers of lung metastatic nodules (**g**). (**c**) Representative images of primary tumors. (**e**) Tumor volume was measured at the indicated days. NS, not significant; $^{*}P < 0.05$, $^{***}P < 0.001$ for rWISP-1 + DMSO vs. Vehicle + DMSO; $^{+}P < 0.05$, $^{+++}P < 0.001$ for rWISP-1 + DMSO vs. rWISP-1 + Fludarabine, Analysis of variance with Tukey's post hoc test. The data are presented as the mean ± standard error of results from 5 mice per group. (**f**) Representative images of lungs with or without metastatic tumor nodules. The yellow dashed circles indicate lung metastatic nodules. (**h**) Numbers of mice with (w/) and without (w/o) visibly determined metastases (Met). (**i**, **k**, **m**) Representative confocal images of primary tumor sections stained with an anti-Ki67 antibody (red; **i**), an anti-cleaved caspase-3 antibody (green; **k**), anti-phophorylated STAT1 (green; **m**), an anti-326 antibody (green or red), and DAPI (blue). ROI – Merge panels show high-magnification of regions of interest as indicated by white squares in Merge panels (**m**). Original magnification: ×40. Scale bars = 100 μm. (**j**, **l**, **n**) Quantification of $Ki67^{+}$, cleaved caspase-3^{+} cells, and relative fluorescence intensity of phosphorylated STAT1 staining among $CD326^{+}$ cells. The data are represented as the means ± standard errors from three mice per group. NS, not significant; $^{*}P < 0.05$, $^{***}P < 0.001$. Analysis of variance with Tukey's post hoc test. The data are from one experiment representative of three independent experiments with similar results (**i**, **k**, **m**)

Conclusion

Our study indicates that the direct interaction between CAFs and apoptotic cancer cells impedes lung cancer cell proliferation and promoted apoptosis through the WISP-1-integrin αvβ3-STAT1 signaling pathway. Moreover, injecting ApoSQ-CAF CM potently suppresses tumor growth by targeting lung cancer cells through the WISP-1-STAT1 signaling axis. The bioinformatics analyses for clinical relevance highlight the translational potential of modulating the TME through the reprogramming of *h*CAFs by apoptotic lung cancer cells to suppress tumor growth. Therefore, developing cell-free therapy, including CM from CAFs exposed to apoptotic cancer cells, and incorporating components like WISP-1 or targeted therapies focused on its upstream regulators, holds promise for establishing a novel therapeutic paradigm against lung cancer and possibly other malignant tumors.

Abbreviations

TME	Tumor microenvironment
CAFs	Cancer-associated fibroblasts
hCAFs	Human CAFs
WISP-1	Wnt-induced signaling protein 1
STAT1	Signal transducer and activator of transcription 1
CM	Conditioned medium
rWISP-1	Recombinant WISP-1
PI	Propidium iodide
FBS	Fetal bovine serum
PBS	Phosphate-buffered saline
BSA	Bovine serum albumin
CCK-8	Cell counting Kit-8
CoIP	Co-immunoprecipitation
qRT-PCR	Quantitative reverse transcription-PCR
ELISA	Enzyme-linked immunosorbent assay
ApoSQ	Apoptotic 344SQ cells
NecSQ	Necrotic 344SQ cells
ApoA	Apoptotic A549 cells
NecA	Necrotic A549 cells
ApoH	Apoptotic HCT116 cells
NecH	Necrotic HCT116 cells
ApoL	Apoptotic LoVo cells
NecL	Necrotic LoVo cells
PCNA	Proliferating cell nuclear antigen
PARP	Poly ADP-ribose polymerase

Supplementary Information

The online version contains supplementary material available at https://doi.org/10.1186/s12964-025-02094-2.

Supplementary Material 1

Supplementary Material 2

Acknowledgements

The authors thank Dr. J.M. Kurie (University of Texas MD Anderson Cancer Center, USA) for providing 344SQ cells and syngeneic (129/Sv) mice.

Author contributions

SK performed mainly in vitro cell proliferation experiments and analyzed data. KY performed mainly in vivo experiments and analyzed data. KK performed mainly in vitro apoptosis experiments and analyzed data. HJK and DK performed in vitro cell proliferation and apoptosis in part. JC and YHA analyzed and interpreted the data. JLK directed and designed the study, analyzed data, and wrote the paper. All authors have read and approved the article.

Funding

This work was supported by the National Research Foundation of Korea (NRF) grants (2020R1A5A2019210 and 2023R1A2C2003185) funded by the Korean Ministry of Science and ICT.

Data availability

No datasets were generated or analysed during the current study.

Declarations

Ethics approval and consent to participate

All proposed mouse studies were approved by the Institutional Animal Care and Use Committee (IACUC) of Ewha Womans University College of Medicine (EWHA MEDIACUC 22-015-3). No human subjects.

Consent for publication

Not applicable.

Competing interests

The authors declare no competing interests.

Conflict of interest

The authors declare that they have no competing interests.

Author details

[1]Department of Physiology, College of Medicine, Ewha Womans University, 25 Magokdong-ro 2-gil, Gangseo-gu, Seoul 07804, Korea
[2]Inflammation-Cancer Microenvironment Research Center, College of Medicine, Ewha Womans University, Seoul 07804, Korea

[3]Department of Biochemistry, College of Medicine, Ewha Womans University, Seoul 07985, Korea
[4]Department of Molecular Medicine, College of Medicine, Ewha Womans University, Seoul 07985, Korea

Received: 30 August 2024 / Accepted: 8 February 2025
Published online: 18 February 2025

References

1. Sung H, Ferlay J, Siegel RL, Laversanne M, Soerjomataram I, Jemal A, et al. Global cancer statistics 2020: GLOBOCAN estimates of incidence and mortality worldwide for 36 cancers in 185 countries. CA Cancer J Clin. 2021;71:209–49.
2. Siegel RL, Miller KD, Jemal A. Cancer statistics, 2019. CA Cancer J Clin. 2019;69:7–34.
3. Gazdar AF, Schiller JH. Predictive and prognostic factors for non–small cell lung cancer potholes in the road to the promised land. J Natl Cancer Inst. 2011;103:1810–11.
4. Meurette O, Mehlen P. Notch signaling in the tumor microenvironment. Cancer Cell. 2018;4:36–548.
5. Öhlund D, Elyada E, Tuveson D. Fibroblast heterogeneity in the cancer wound. J Exp Med. 2014;211:1503–23.
6. Tao L, Huang G, Song H, Chen Y, Chen L. Cancer associated fibroblasts: an essential role in the tumor microenvironment. Oncol Lett. 2017;14:2611–20.
7. Sahai E, Astsaturov I, Cukierman E, DeNardo DG, Egeblad M, Evans RM, et al. A framework for advancing our understanding of cancerassociated fibroblasts. Nat Rev Cancer. 2020;20:174–86.
8. Gieniec KA, Butler LM, Worthley DL, Woods SL. Cancer-associated fibroblasts-heroes or villains? Br J Cancer. 2019;121:293–302.
9. Poon IKH, Lucas CD, Rossi AG, Ravichandran KS. Apoptotic cell clearance: basic biology and therapeutic potential. Nat Rev Immunol. 2014;4:166–80.
10. Vaught DB, Stanford JC, Cook RS. Efferocytosis creates a tumor microenvironment supportive of tumor survival and metastasis. Cancer Cell Microenviron. 2015;2:e666.
11. Werfel TA, Cook RS. Efferocytosis in the tumor microenvironment. Semin Immunopathol. 2018;40:545–54.
12. Kim HJ, Yang K, Kim K, Lee YJ, Lee S, Ahn SY, et al. Reprogramming of cancer-associated fibroblasts by apoptotic cancer cells inhibits lung metastasis via Notch1-WISP-1 signaling. Cell Mol Immunol. 2022;19:1373–91.
13. Evan GI, Vousden KH. Proliferation, cell cycle and apoptosis in cancer. Nature. 2001;411:342–8.
14. Lee S, Hong JH, Kim JS, Yoon JS, Chun SH, Hong SA, et al. Cancer-associated fibroblasts activated by miR-196a promote the migration and invasion of lung cancer cells. Cancer Lett. 2021;508:92–103.
15. Kim D, Kim JS, Cheon I, Kim SR, Chun SH, Kim JJ, et al. Identification and characterization of cancer-associated fibroblast subpopulations in lung adenocarcinoma. Cancers (Basel). 2022;14:3486–502.
16. Kim YB, Ahn YH, Jung JH, Lee YJ, Lee JH, Kang JH. Programming of macrophages by UV-irradiated apoptotic cancer cells inhibits cancer progression and lung metastasis. Cell Mol Immunol. 2019;16:851–67.
17. Zhao Y, Ma C, Chen C, Li S, Wang Y, Yang T, et al. STAT1 contributes to microglial/macrophage inflammation and neurological dysfunction in a mouse model of traumatic brain injury. J Neurosci. 2022;42:7466–81.
18. Sun L, Han X, Egeblad M. Isolation of mouse mammary carcinoma-derived macrophages and cancer cells for co-culture assays. STAR Protoc. 2022;3:101833.
19. Pankova D, Chen Y, Terajima M, Schliekelman MJ, Baird BN, Fahrenholtz M, et al. Cancer-associated fibroblasts induce a collagen cross-link switch in tumor stroma. Mol Cancer Res. 2016;14:287–95.
20. Lidia A, Sara P, Gabriella R, Francesco N, Valeria P. STAT1 and STAT3 in tumorigenesis: A matter of balance. JAK-STAT. 2012;1:65–72.
21. Hix LM, Karavitis J, Khan MW, Shi YH, Khazaie K, Zhang M. Tumor STAT1 transcription factor activity enhances breast tumor growth and immune suppression mediated by myeloid-derived suppressor cells. J Biol Chem. 2013;288:11676–88.
22. Engeland K. Cell cycle regulation: p53-p21-RB signaling. Cell Death Differ. 2022;29:946–60.
23. Gomez-Manzano C, Fueyo J, Kyritsis AP, Steck PA, Levin VA, Alfred Yung WK, et al. Characterization of p53 and p21 functional interactions in glioma cells en route to apoptosis. J Nat Cancer Inst. 1997;89:16.
24. Li J, Ye L, Owen S, Weeks HP, Zhang Z, Jiang WG. Emerging role of CCN family proteins in tumorigenesis and cancer metastasis (review). Int J Mol Med. 2015;36:1451–63.
25. Lau LF. Cell surface receptors for CCN proteins. J Cell Commun Signal. 2016;10:121–7.
26. Salcher S, Sturm G, Horvath L, Untergasser G, Kuempers C, Fotakis G, et al. High-resolution single-cell atlas reveals diversity and plasticity of tissue-resident neutrophils in non-small cell lung cancer. Cancer Cell. 2022;40:1503–20.
27. Kovarik P, Mangold M, Ramsauer K, Heidari H, Steinborn R, Zotter A, et al. Specificity of signaling by STAT1 depends on SH2 and C-terminal domains that regulate Ser727 phosphorylation, differentially affecting specific target gene expression. EMBO J. 2001;20:91–100.
28. Gregory CD, Dransfield I. Apoptotic tumor cell-derived extracellular vesicles as important regulators of the onco-regenerative niche. Front Immunol. 2018;9:111.
29. Lindsay J, Esposti MD, Gilmore AP. Bcl-2 proteins and mitochondria–specificity in membrane targeting for death. Biochim Biophys Acta. 2011;1813:532–9.
30. Oltvai ZN, Milliman CL, Korsmeyer SJ. Bcl-2 heterodimerizes in vivo with a conserved homolog, Bax, that accelerates programmed cell death. Cell. 1993;74:609–19.
31. Yang E, Korsmeyer SJ. Molecular thanatopsis: a discourse on the BCL2 family and cell death. Blood. 1996;88:386–401.
32. Li J, Yuan J. Caspases in apoptosis and beyond. Oncogene. 2008;27:6194–206.
33. Avalle L, Pensa S, Regis G, Novelli F, Poli V. STAT1 and STAT3 in tumorigenesis: A matter of balance. JAK-STAT. 2012;1:65–72.
34. Zhang Y, Zhang Y, Yun H, Lai R, Su M. Correlation of STAT1 with apoptosis and cell-cycle markers in esophageal squamous cell carcinoma. PLoS ONE 2014;9: e113928.
35. Shao H, Cai L, Moller M, Issac B, Zhang L, Owyong M, et al. Notch1-WISP-1 axis determines the regulatory role of mesenchymal stem cell-derived stromal fibroblasts in melanoma metastasis. Oncotarget. 2016;7:79262–73.
36. Soon LL, Yie TA, Shvarts A, Levine AJ, Su F, Tchou-Wong KM. Overexpression of WISP-1 down-regulated motility and invasion of lung cancer cells through inhibition of rac activation. J Biol Chem. 2003;278:11465–70.
37. Liu Y, Song Y, Ye M, Hu X, Wang ZP, Zhu X. The emerging role of WISP proteins in tumorigenesis and cancer therapy. J Transl Med. 2019;17:28.
38. Margalit O, Eisenbach L, Amariglio N, Kaminski N, Harmelin A, Pfefer R, et al. Overexpression of a set of genes, including WISP-1, common to pulmonary metastases of both mouse D122 Lewis lung carcinoma and B16-F10.9 melanoma cell lines. Br J Cancer. 2003;89:314–9.
39. Chen PP, Li WJ, Wang Y, Zhao S, Li DY, Feng LY, et al. Expression of Cyr61, CTGF, and WISP-1 correlates with clinical features of lung cancer. PLoS ONE. 2007;2:e534.
40. Paolillo M, Serra M, Schinelli S. Integrins in glioblastoma: still an attractive target? Pharmacol Res. 2016;113:55–61.
41. Barczyk M, Carracedo S, Gullberg D, Integrins. Cell Tissue Res. 2010;339:269–80.
42. Mas-Moruno C, Rechenmacher F, Kessler H. Cilengitide: the first antiangiogenic small molecule drug candidate design, synthesis and clinical evaluation. Anticancer Agents Med Chem. 2010;10:753–68.
43. Reynolds LE, Wyder L, Lively JC, Taverna D, Robinson SD, Huang X, et al. Enhanced pathological angiogenesis in mice lacking beta3 integrin or beta3 and beta5 integrins. Nat Med. 2002;8:27–34.
44. Kim KB, Prieto V, Joseph RW, Diwan AH, Gallick GE, Papadopoulos NE, et al. A randomized phase II study of cilengitide (EMD 121974) in patients with metastatic melanoma. Melanoma Res. 2012;22:294–301.
45. Manegold C, Vansteenkiste J, Cardenal F, Schuette W, Woll PJ, Ulsperger E, et al. Randomized phase II study of three doses of the integrin inhibitor cilengitide versus docetaxel as second-line treatment for patients with advanced non-small-cell lung cancer. Invest New Drugs. 2013;31:175–82.
46. Stupp R, Hegi ME, Gorlia T, Erridge SC, Perry J, Hong YK, et al. Cilengitide combined with standard treatment for patients with newly diagnosed glioblastoma with methylated MGMT promoter (CENTRIC EORTC 26071– 22072

study): a multicentre, randomised, open-label, phase 3 trial. Lancet Oncol. 2014;15:1100–08.
47. Chang CW, Tsai WH, Chuang WJ, Lin YS, Wu JJ, Liu CC, et al. Procaspase 8 and Bax are up-regulated by distinct pathways in streptococcal pyrogenic exotoxin B-induced apoptosis. J Biol Chem. 2009;284:33195–205.

Publisher's note